AD_____

Award Number:
W81XWH-08-1-0117

TITLE:
Novel Optical Methods for Identification, Imaging, and Preservation of the Cavernous Nerves Responsible for Penile Erections during Prostate Cancer Surgery

PRINCIPAL INVESTIGATOR:
Nathaniel M. Fried, Ph.D.

CONTRACTING ORGANIZATION:
University of North Carolina,Charlotte
Charlotte, NC 28223-0001

REPORT DATE:
March 2011

TYPE OF REPORT:
Annual

PREPARED FOR: U.S. Army Medical Research and Materiel Command
Fort Detrick, Maryland 21702-5012

# REPORT DOCUMENTATION PAGE

*Form Approved*
*OMB No. 0704-0188*



| **1. REPORT DATE** *(DD-MM-YYYY)* | **2. REPORT TYPE** | **3. DATES COVERED** *(From - To)* |
|---|---|---|
| 01-03-2011 | Annual | 1 Mar 2010 – 28 Feb 2011 |

**4. TITLE AND SUBTITLE**
Novel Optical Methods for Identification, Imaging, and Preservation of the Cavernous Nerves Responsible for Penile Erections During Prostate Cancer Surgery

**5a. CONTRACT NUMBER**

**5b. GRANT NUMBER**
W81XWH-08-1-0117

**5c. PROGRAM ELEMENT NUMBER**

**6. AUTHOR(S)**
Nathaniel M. Fried, Ph.D.
nmfried@uncc.edu

**5d. PROJECT NUMBER**

**5e. TASK NUMBER**

**5f. WORK UNIT NUMBER**

**7. PERFORMING ORGANIZATION NAME(S) AND ADDRESS(ES)**
University of North Carolina, Charlotte

Charlotte, NC 28223-0001

**8. PERFORMING ORGANIZATION REPORT NUMBER**

**9. SPONSORING / MONITORING AGENCY NAME(S) AND ADDRESS(ES)**
U.S. Army Medical Research
and Materiel Command
Fort Detrick, MD 21702-5012

**10. SPONSOR/MONITOR'S ACRONYM(S)**

**11. SPONSOR/MONITOR'S REPORT NUMBER(S)**

**12. DISTRIBUTION / AVAILABILITY STATEMENT**
Approved for public release; distribution unlimited

**13. SUPPLEMENTARY NOTES**

**14. ABSTRACT**
There is wide variability in sexual potency rates (9-86%) after prostate cancer surgery due to a limited understanding of the location of the cavernous nerves, which are responsible for erectile function. Advances in identification and preservation of these nerves would result in improved postoperative potency and patient quality of life. We hypothesize that application of 3 optical technologies for identification, imaging, and preservation of the nerves during prostate surgery will result in improved sexual function: (1) Laser nerve stimulation for identification, (2) optical coherence tomography (OCT) for nerve imaging, and (3) precise laser prostate dissection for nerve preservation. In Year 3, we compared time-domain and fourier-domain OCT for prostate imaging. We also developed a new approach to stimulation of prostate nerves using continuous-wave laser radiation, a new laser wavelength, and an all-single-mode fiber system, which resulted in faster stimulation and a more compact, less expensive system. We published 2 manuscripts and 3 conference proceedings on this work.

**15. SUBJECT TERMS**
Laser Nerve Stimulation; Optical Coherence Tomography; Cavernous Nerves

| **16. SECURITY CLASSIFICATION OF:** | | | **17. LIMITATION OF ABSTRACT** | **18. NUMBER OF PAGES** | **19a. NAME OF RESPONSIBLE PERSON** |
|---|---|---|---|---|---|
| **a. REPORT** | **b. ABSTRACT** | **c. THIS PAGE** | | | USAMRMC |
| U | U | U | UU | 48 | **19b. TELEPHONE NUMBER** *(include area code)* |

# TABLE OF CONTENTS

# INTRODUCTION

One of the greatest challenges of prostate cancer surgery is preservation of sexual function after surgery. There is wide variability in reported post-operative potency rates (9 - 86%). This variability may be due, in part, to our limited understanding of the location, extent, and course of the cavernous nerves, which are responsible for erectile function. Because of the close proximity of the nerves to the surface of the prostate, they are at risk of damage during surgical dissection and removal of a cancerous prostate gland. In addition, their microscopic nature makes it difficult to predict the true course and location of these nerves from one individual patient to another. Improvements in identification, imaging, and visualization of these nerves will likelyimprove the consistency of nerve preservation and postoperative potency, leading to an improved quality of life for patients.

We hypothesize that the application of novel optical technologies for identification, imaging, and preservation of the cavernous nerves during prostate cancer surgery will result in improved sexual function. We intend to test three complementary optical technologies: Non-contact laser stimulation for identification of the cavernous nerves, high-resolution imaging of the cavernous nerves using optical coherence tomography (OCT), and rapid, precise, and hemostatic dissection of the prostate from the cavernous nerves using a KTP laser.

Year 1 was devoted to optimization of the laser nerve stimulation parameters and direct comparison with conventional electrical nerve stimulation. We completed these tasks ahead of schedule, and started work on some of the Year 2 aims as well, such as assembly of a laparoscopic laser nerve stimulation probe, and improving the image quality of OCT for differentiating the cavernous nerves from the prostate gland. The Year 1 work resulted in the publication of 2 manuscripts, 5 conference proceedings papers, and 3 abstracts, as stated in the Year 1 Report.

In Year 2, we continued development and testing of the laparoscopic laser nerve stimulation probe, incorporating laser beam collimation and laser beam shaping methods into the device. This resulted in faster and stronger stimulation at shorter durations than previously reported using the conventional probe design. We also measured the optical properties of the prostate gland at several near-infrared laser wavelengths for potential use OCT systems. Our study found improved optical penetration depth at 1064 nm in comparison with the conventional 1310 nm wavelength currently used in OCT. Finally, we combined the application of three complementary image processing algorithms (denoising, segmentation, and edge detection) to OCT images of the rat prostate and cavernous nerves to improve the image metrics (SNR and CNR) and imaging depth. During Year 2, we published 2 manuscripts, 5 conference proceedings, and 1 abstract, as stated in Year 2 Report.

During Year 3, we performed an OCT study comparing time-domain and fourier-domain OCT for imaging of prostate nerves and discovered that TD-OCT, although slower, provides deeper imaging through prostate tissues. We also developed a more compact, less expensive method for performing infrared stimulation of the prostate nerves using continuous-wave (CW) laser radiation. We then took this approach one step further, by designing an all-single-mode fiber configuration for optical nerve stimulation that eliminates the use of bulk optical components and alignment and maintenance issues. In summary, during Year 3, we published 2 manuscripts and 3 conference proceedings. We presented our results at the International Symposium for Biomedical Optics (SPIE) in January, 2011.

We have requested and been granted a 1-year no-cost extension for this project. In year 4, we plan to complete some of the Year 3 tasks associated with rapid, precise, and hemostatic dissection of the prostate from the cavernous nerves using a KTP laser.

# BODY

## Study #1: Time-domain versus Fourier-domain Optical Coherence Tomography of the Prostate Nerves

### Introduction

Theoretical comparisons of detection performance for Fourier domain (FD) and time domain (TD) optical coherence tomography (OCT) have been previously reported. In this study we compare several image quality metrics including signal-to-noise ratio (SNR), contrast-to-noise ratio (CNR), and equivalent number of looks (ENL) for TD-OCT and FD-OCT images taken of the rat prostate, in vivo.

### Results

Nine sample images of the cavernous nerves at different orientations (longitudinal, oblique, and cross-sectional) along the surface of the rat prostate were acquired using TD- an FD-OCT systems. Figure 1 (a,c,e) shows the denoised TD-OCT images of the cavernous nerves and the prostate. Representative histologic sections were processed for comparison, Fig 1 (b,d,f). Figure 2 corresonds to the FD-OCT images before and after denoising.

The values of CNR, ENL, and SNR for nine FD-OCT and TD-OCT images are shown in Table 1. The values were measured for both original and denoised images.

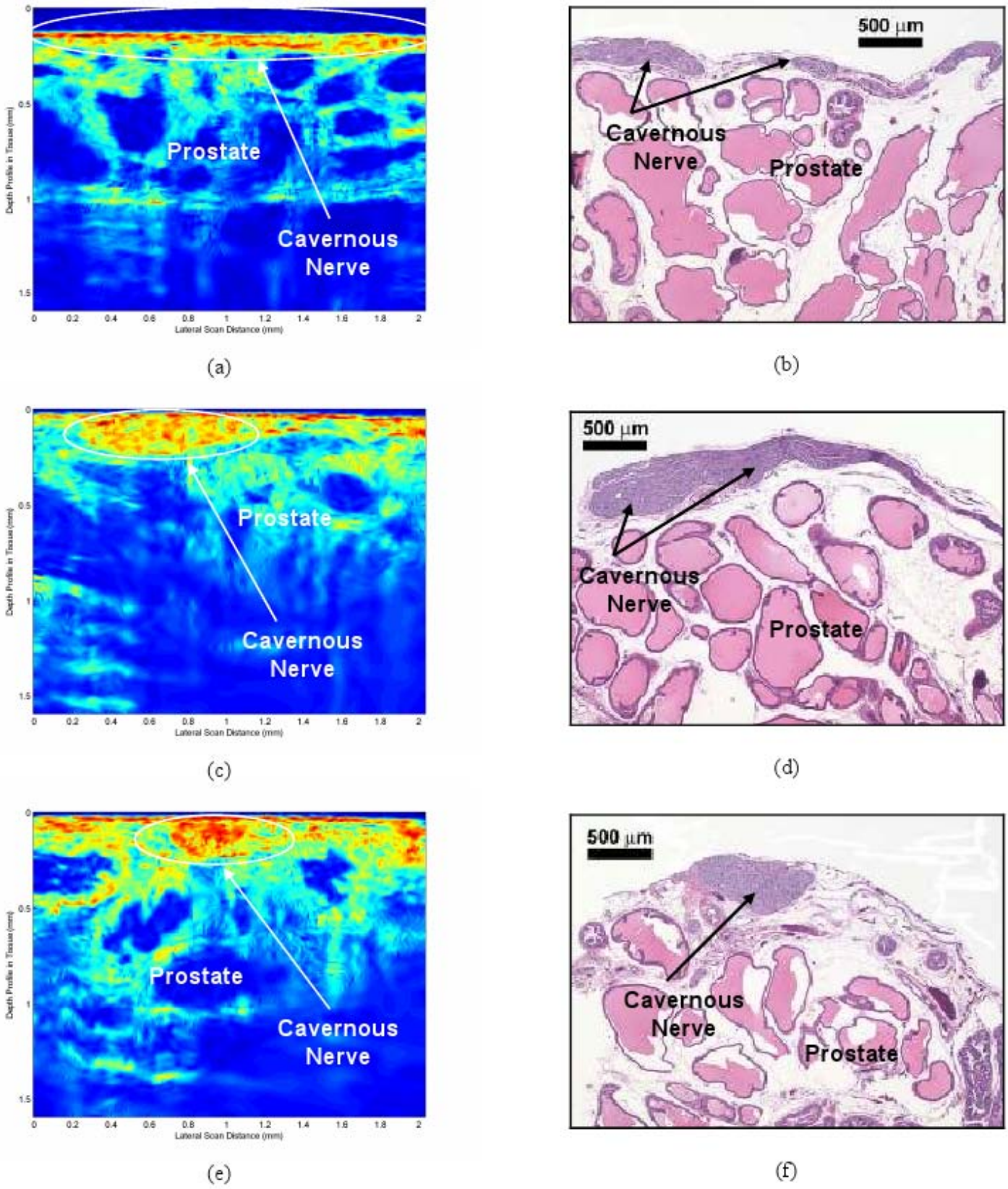


**Figure 1.** TD-OCT and corresponding histologic images of the rat cavernous nerve. (a,b) Longitudinal section; (c,d) Oblique section; (e,f) Cross-section.

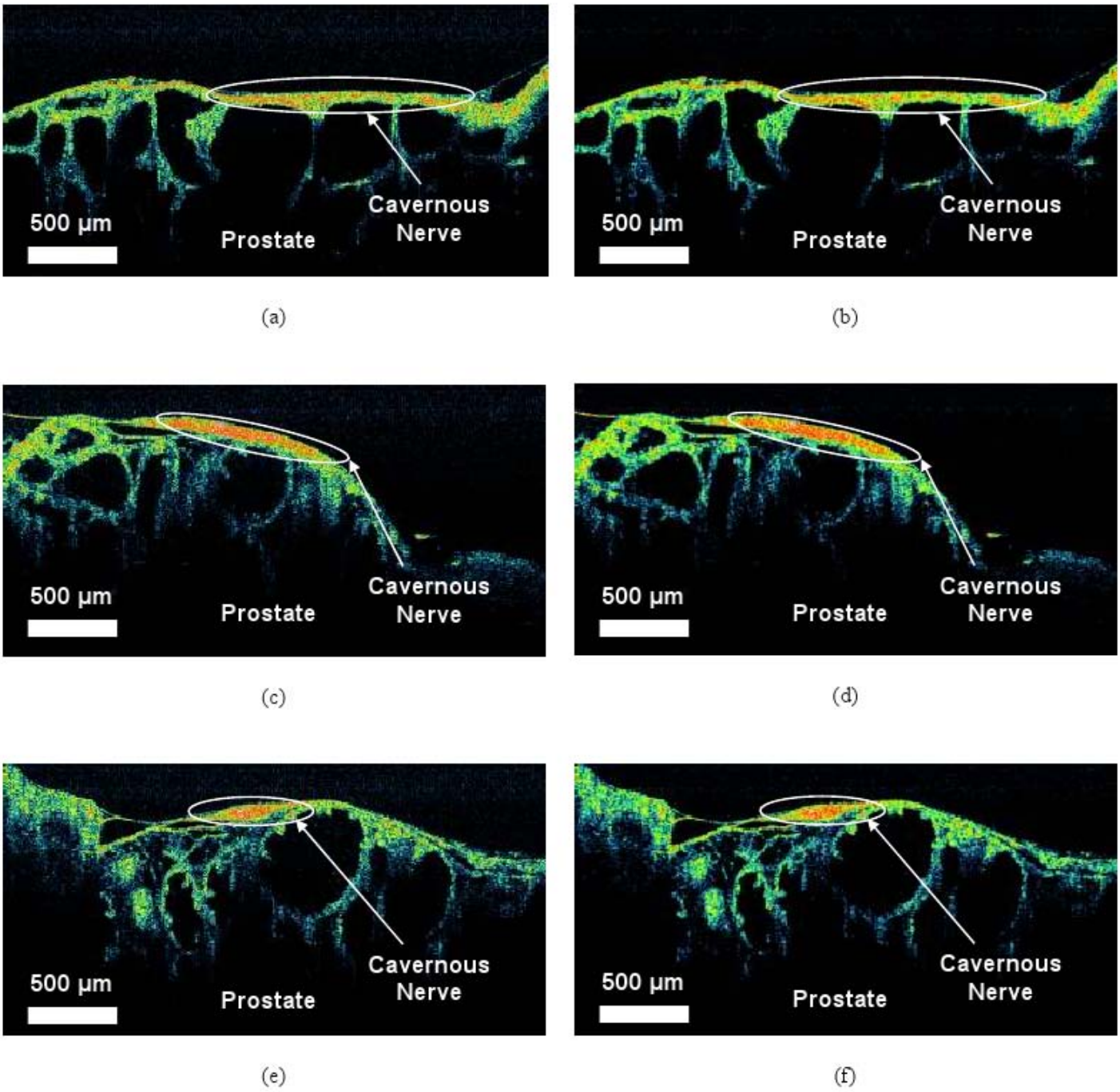


**Figure 2.** FD-OCT images of the rat cavernous nerve: (a,b) Longitudinal section; (c,d) Cross-section; (e,f) Oblique section. (a,c,e) before; (b,d,f) after denoising.

**Table 1.** Image quality metrics for FD-OCT and TD-OCT imaging of the prostate gland.

| | | FD-OCT | | | TD-OCT | | |
|---|---|---|---|---|---|---|---|
| **No.** | **Image** | **CNR (dB)** | **ENL** | **SNR (dB)** | **CNR (dB)** | **ENL** | **SNR (dB)** |
| 1 | Original | 9.53 | 59.4 | 23.26 | 3.33 | 1168.6 | 23.36 |
| | Denoised | 17.07 | 1431.2 | 34.15 | 5.63 | 1490.9 | 27.13 |
| 2 | Original | 9.50 | 296.6 | 21.71 | 9.09 | 1420.9 | 27.50 |
| | Denoised | 15.64 | 695.0 | 31.57 | 12.03 | 1932.4 | 45.27 |
| 3 | Original | 10.01 | 100.9 | 23.49 | 9.11 | 1276.9 | 27.99 |
| | Denoised | 17.16 | 630.9 | 34.92 | 11.48 | 1609.9 | 46.06 |
| 4 | Original | 7.58 | 117.9 | 19.96 | 11.96 | 1580.4 | 28.07 |
| | Denoised | 12.23 | 1290.7 | 27.88 | 14.08 | 1866.3 | 35.64 |
| 5 | Original | 10.05 | 102.1 | 23.37 | 7.67 | 1621.7 | 26.76 |
| | Denoised | 17.26 | 1376.2 | 36.71 | 11.39 | 2442.9 | 47.60 |
| 6 | Original | 9.74 | 143.5 | 22.52 | 7.05 | 893.2 | 28.61 |
| | Denoised | 16.07 | 550.3 | 36.54 | 8.86 | 1080.6 | 45.21 |
| 7 | Original | 8.29 | 127.9 | 21.00 | 9.50 | 1974.1 | 25.62 |
| | Denoised | 13.53 | 1671.3 | 33.02 | 13.56 | 2894.8 | 43.90 |
| 8 | Original | 9.08 | 120.9 | 20.77 | 12.44 | 3575.3 | 26.88 |
| | Denoised | 15.10 | 574.4 | 30.18 | 19.32 | 7580.6 | 43.42 |
| 9 | Original | 8.87 | 61.7 | 22.46 | 4.67 | 1014.1 | 25.13 |
| | Denoised | 15.91 | 921.4 | 32.74 | 6.90 | 1303.0 | 33.59 |
| **Mean** | **Original** | **9.18** | **125.6** | **22.06** | **8.31** | **1613.9** | **26.65** |
| | **Denoised** | **15.55** | **1015.7** | **33.08** | **11.47** | **2466.8** | **40.87** |

## Conclusions

TD-OCT has distinct advantages for imaging opaque tissues, such as the prostate gland, in applications where imaging penetration depth is important. Denoising is also more effective for TD-OCT compared to FD-OCT with respect to SNR.

## Study #2: Continuous-wave Optical Stimulation of the Prostate Nerves

### Introduction

Recent optical nerve stimulation (ONS) studies by other researchers have focused primarily on the use of laser radiation delivered in pulsed mode and at low pulse repetition rates (2-13 Hz), to avoid thermal build-up and thermal damage to the nerves during long-term stimulation applications. However, our research group is interested in the potential of ONS to be used as an intra-operative diagnostic tool for identification and preservation of the cavernous nerves during prostate cancer surgery. Practical application of ONS would thus require rapid, short-term nerve stimulation for identification of the cavernous nerves. Therefore, for this current study, we chose to explore delivery of the infrared laser radiation to the nerve at significantly higher pulse rates (10-100 Hz) and in CW mode, with the hypothesis that this method may result in a more rapid response for identification of the cavernous nerves.

### Results

Table 2 provides a summary of the results for CW vs. pulsed ONS. The threshold (minimum) pulse energy, incident fluence, average power, total energy, and temperature for successful ONS are reported, along with the ICP response time. The pulse energy and incident fluence for successful ONS were not fixed as previously thought, but rather decreased significantly as the laser pulse rate was increased. The average power to reach stimulation threshold, however, was not dependent on the pulse rate. The ICP response time decreased as the pulse rate was increased from 10-100 Hz, with CW irradiation providing the fastest ICP response time. For the 10 Hz data set, the delayed ICP response actually occurred just after the end of the 15 s laser irradiation time. Finally, successful ONS was observed to be primarily dependent on the time necessary for the nerve to reach a stimulation threshold temperature of 42-45 $^{o}$C, rather than dependent on a specific set of laser parameters.

**Table 2.** Optical nerve stimulation threshold parameters for continuous-wave versus pulsed laser irradiation.

| | Laser Pulse Repetition Rate | | | | | | |
|---|---|---|---|---|---|---|---|
| **Parameter** | **10 Hz** | **20 Hz** | **30 Hz** | **40 Hz** | **50 Hz** | **100 Hz** | **CW** |
| Pulse Energy (mJ): | 4.84 | 2.57 | 1.71 | 1.34 | 0.94 | 0.56 | NA |
| Incident Fluence (J/cm$^2$): | 0.51 | 0.27 | 0.18 | 0.14 | 0.10 | 0.06 | NA |
| Average Power (mW): | 48.4 | 51.3 | 51.2 | 53.6 | 47.2 | 55.5 | 47.3 |
| ICP Response Time (s): | 16.7 ± 1.9 | 14.8 ± 1.3 | 14.5 ± 1.1 | 14.0 ± 0.5 | 12.8 ± 1.3 | 10.9 ± 1.6 | 9.7 ± 0.8 |
| Total Energy until Stim. (J): | 0.73 | 0.76 | 0.74 | 0.75 | 0.60 | 0.60 | 0.46 |
| Temperature ($^{o}$C): | 43.8 ± 1.3 | 42.3 ± 1.1 | 42.3 ± 0.2 | 41.5 ± 0.6 | 44.9 ± 1.2 | 44.7 ± 1.2 | 42.9± 0.3 |

CW optical stimulation of the rat CN is shown in Figure 3. A strong response in the rat penis was observed with ICP increasing from a baseline of 16 mmHg to a peak of 39 mmHg. This response occurred ~ 10 s after laser was turned on, corresponding to the time necessary for the CN to heat up above a threshold temperature of ~ 43 $^{o}$C.

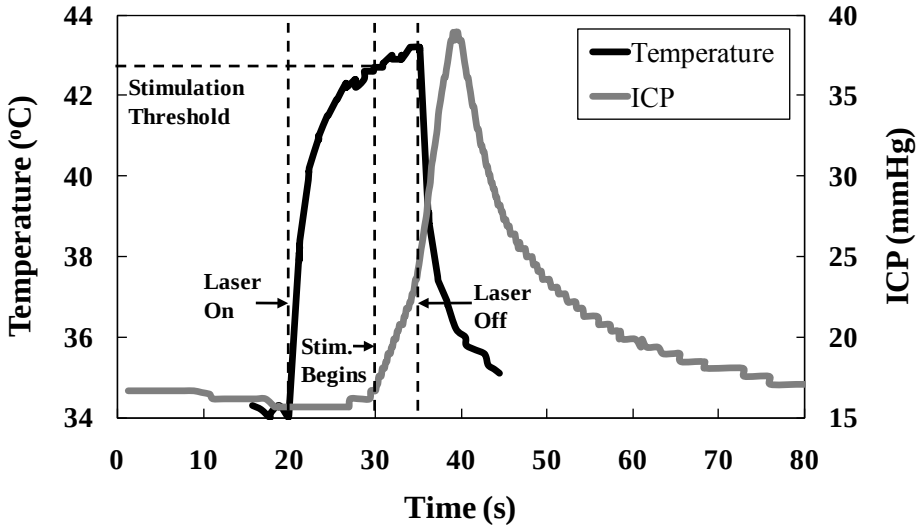


**Figure 3.** CW stimulation of the rat CN (Wavelength = 1870 nm, Spot = 1.1 mm, Power = 47 mW, Total Energy = 0.71 J, Stimulation Time = 15 s). The ICP response in the rat penis begins to increase ~ 10 s after laser irradiation begins (at t = 20 s) and then continues to increase after laser irradiation ends (at t = 35 s). The cavernous nerve reaches a stimulation threshold temperature of ~ 43 $^{o}$C after 10 s of laser irradiation (at t = 30 s), closely corresponding to the onset of the increase in ICP.

## Discussion

Previous studies have demonstrated successful ONS using pulsed infrared laser radiation for applications demanding long-term stimulation, as an alternative to conventional ENS. The purpose of this study was to demonstrate short-term ONS using CW infrared laser radiation for producing a more rapid response, necessary for intra-operative diagnostic applications, such as identification of the CN's during prostate cancer surgery. ICP response time decreased significantly as the laser pulse rate increased and optimal results were observed when the laser was operated in CW mode.

There appears to be a logical explanation for the results summarized in Table 1. CW stimulation produces the fastest ICP response because delivery of the laser radiation in CW mode also produces the fastest increase in temperature from baseline to above the nerve stimulation threshold temperature of ~ 43 $^{o}$C, as compared to pulsed irradiation with a pulse duration of 5 ms and pulse rates of 10-100 Hz.

The results of this study also further confirm that ONS operates primarily based on a photothermal mechanism, in which light energy is converted to heat energy in the nerve, until a sufficient amount of heat is generated to increase the nerve temperature above a threshold value (42-45 $^{o}$C) for activation. A strong correlation was observed between the laser irradiation time necessary to raise the nerve temperature above the stimulation threshold and the onset of ICP response, as shown in Figure 3. Thus, successful ONS was observed to be primarily dependent on the time necessary for the nerve to reach a stimulation threshold temperature for activation, rather than dependent on a specific set of laser parameters.

## Conclusions

Continuous-wave laser irradiation produces faster optical stimulation of the rat cavernous nerve, as measured by an intracavernous pressure response in the penis, than does pulsed irradiation. This may be important in intra-operative diagnostic applications requiring rapid feedback, such as identification of the cavernous nerves and preservation of erectile function during prostate cancer surgery.

## Study #3: All-single-mode System for Optical Stimulation of Prostate Nerves

### Introduction

In our laboratory, we have studied ONS of the rat CN, *in vivo*, as a standard pre-clinical animal model for optical stimulation of the prostate cavernous nerves. Successful optical stimulation of the rat CN using both pulsed and continuous-wave (CW) infrared laser radiation has been previously reported. CW infrared laser irradiation during optical stimulation of neural tissue has been shown to result in faster deposition of energy into the nerve, thus producing a more rapid intracavernous pressure (ICP) response. This approach may also allow the use of a less expensive and more compact laser system (e.g. diode laser) for potential diagnostic applications. In all of our previous studies, the experimental setup utilized a relatively expensive Thulium fiber laser, a complex configuration of bulk optical components, and a multimode fiber optic delivery system. This setup introduced a number of limitations, including high cost optical components, periodic maintenance for optical alignment and cleaning, and a larger and more expensive ONS system.

In this current study, we utilize a compact and inexpensive pigtailed single-mode diode laser, an all-single-mode fiber (SMF) system design, and fiber optic beam shaping methods for ONS in a rat CN model, *in vivo*. The results described here define a therapeutic window for safe, reliable**,** and reproducible short-term optical stimulation of the CN, which may lead to the development of an intra-operative diagnostic system for identification and preservation of the cavernous nerves, which are responsible for erectile function, during prostate cancer surgery.

### Results

A summary of the ONS results comparing both the Gaussian and flat-top fiber optic probes is provided in Table 3. Rapid ICP response times averaging 4-5 s were recorded using both probes. This rapid ICP response is critical for potential diagnostic ONS applications. Near the optical stimulation threshold, comparable ICP response times of approximately 13 s were also observed. The minimum incident power needed to stimulate the CN was approximately 30 mW, corresponding to an irradiance of 4 W/cm$^2$ for the 1-mm-diameter spot size used in these studies.

**Table 3.** Comparison of threshold ONS parameters for Gaussian and flat-top beam profiles.

| Parameter | Gaussian | Flat-top |
|---|---|---|
| Fastest ICP response time (s): | 3.8 $\pm$ 0.5 | 4.8 $\pm$ 0.9 |
| Threshold ICP response time (s): | 12.7 $\pm$ 1.0 | 13.0 $\pm$ 0.9 |
| Power to stimulate (mW): | 28.3 $\pm$ 5.2 | 33.8 $\pm$ 2.5 |
| Irradiance to stimulate (W/cm$^2$): | 3.6 $\pm$ 0.7 | 3.9 $\pm$ 0.3 |
| Temperature to stimulate ($^o$C): | 41.3 $\pm$ 1.3 | 41.2 $\pm$ 0.6 |
| Power to damage nerve (mW): | 55.0 $\pm$ 7.5 | |
| Irradiance to damage nerve (W/cm$^2$): | 7.0 $\pm$ 1.0 | |
| Temperature to damage nerve ($^o$C): | 48.5 $\pm$ 1.1 | |

Successful optical stimulation of the rat CN was achieved at nerve temperatures of ~ 41 $^o$C. There was an upper stimulation threshold temperature of about 48 $^o$C corresponding to an incident power of ~ 55 mW and an irradiance of 7 W/cm$^2$ for thermal damage to the nerve. Such nerve damage was noted by both visual observation of the nerve surface under magnification as well as a notable decay in both the ICP response time and magnitude with repeated stimulations.

Figure 4 shows strong ICP responses obtained in the rat penis using both Gaussian and flat-top fiber optic probes when the rat CN was irradiated with a laser power significantly above the stimulation threshold but below the thermal damage threshold for a period of 15 s. ICP increased from a baseline of 5-10 mmHg to a peak of approximately 50 mmHg during ONS. This response was observed about 3-4 s after laser irradiation began, corresponding to the time necessary to elevate the CN temperature above a threshold temperature of approximately 42 $^{o}$C for these experiments. The maximum temperature on the CN surface was measured to be about 45 $^{o}$C at the end of stimulation, significantly below the damage threshold temperature of approximately 48 $^{o}$C. It should be noted that the shape and magnitude of the ICP response curve varies significantly among rats, and is dependent on anatomical and physiological parameters (such as nerve dimensions and blood pressure) beyond the control of the ONS parameters. Nevertheless, for the purposes of our study, any ICP response measured during ONS which is significantly above the baseline (noise level) may serve as a reliable indicator for positive identification of the CN during prostate cancer surgery. Thus, the ICP signal-to-noise ratio (SNR) of 5:1 (50 mmHg signal / 10 mmHg baseline) shown here provides a more than sufficient response.

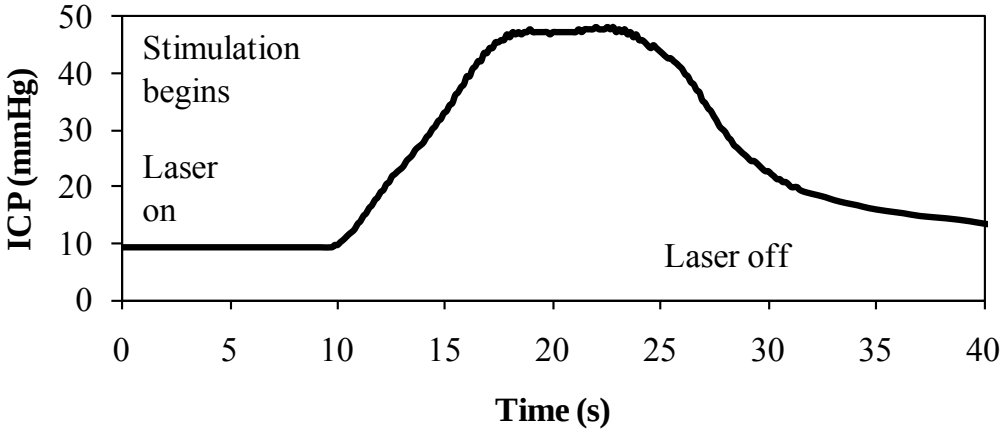


(a) Gaussian beam profile

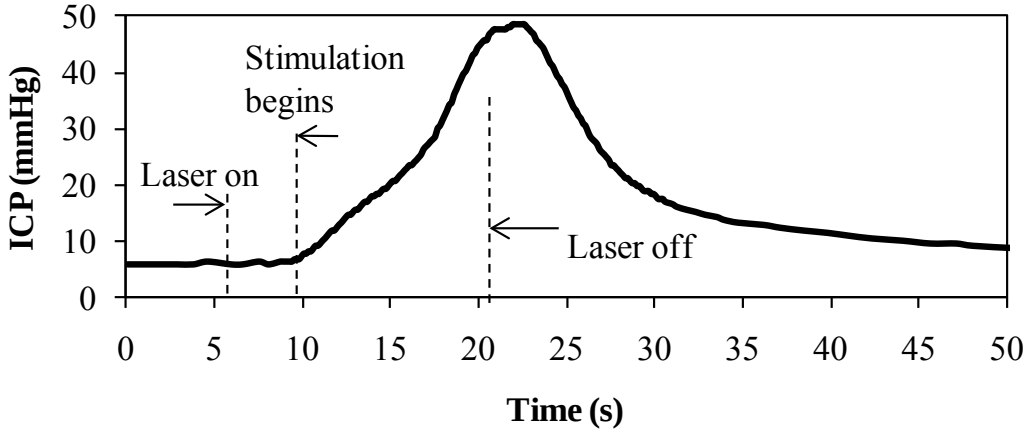


(b) Flat-top beam profile

**Figure 4.** (a) Intracavernous pressure (ICP) response as a function of time for optical stimulation of the rat CN with a Gaussian spatial beam profile (wavelength = 1455 nm, spot diameter = 1 mm, power = 50 mW, total energy = 0.75 J and stimulation time = 15 s); (b) Intracavernous pressure (ICP) response as a function of time for optical stimulation of the rat CN with a flat-top spatial beam profile (wavelength = 1455 nm, spot diameter = 1.1 mm, power = 51 mW, total energy = 0.77 J and stimulation time = 15 s).

## Discussion

Optical nerve stimulation (ONS) using infrared laser radiation has been previously studied as a potential alternative to electrical nerve stimulation (ENS). However, the use of bulk optical components and high-cost infrared lasers (e.g. Holmium:YAG and Thulium fiber lasers) in some of these studies may represent significant hurdles for translation of ONS into use in the clinic. The use of diode lasers with multimode spatial beam profiles coupled to multimode optical fibers for delivery of the laser radiation during ONS may also introduce unnecessary irregularities in the laser beam intensity and difficulty in alignment of the laser beam with the nerve, potentially compromising the safety and consistency of ONS.

This study demonstrates that an all-single-mode-fiber design can be used with a compact and inexpensive infrared diode laser for reproducible, safe, short-term, continuous-wave optical stimulation of the prostate cavernous nerves. ONS using this all-single-mode-fiber configuration provides several advantages: it eliminates the packing complexities encountered during integration of bulk optical components and fiber optics, and it also reduces the maintenance and manufacturing costs of the ONS system.

Although the results in Table 3 demonstrate that there is not a significant difference between the Gaussian and flat-top fiber optic probes in terms of the ONS operating parameters, the flat-top probe definitely allowed simplified alignment of the laser beam with the microscopic nerve, thus providing a more uniform irradiance of the nerve surface and potentially avoiding thermal damage to the nerve from hotspots in the laser spatial beam profile. This feature may prove critical in other applications where the microscopic nerve and laser spot diameter are even smaller and more difficult to co-align.

## Conclusions

An all-single-mode-fiber design for optical stimulation of the rat cavernous nerve, using CW infrared laser radiation, was successfully tested. This approach has several advantages, including lower cost, elimination of alignment and maintenance issues, and improved spatial beam profile for simplified alignment of the laser beam with the microscopic nerve. With further development, this ONS system may be useful for identification and preservation of the cavernous nerves, which are responsible for erectile function, during prostate cancer surgery.

# KEY RESEARCH ACCOMPLISHMENTS

- Two different OCT systems (time-domain and Fourier-domain) were compared using image metrics (SNR, CNR, and equivalent number of looks). Although the TD-OCT system has a slower image acquisition time, it was found to have superior signal-to-noise ratio for deeper imaging of the prostate gland.

- A continuous-wave (CW) method of optically stimulating the prostate nerves was developed, resulting in faster stimulation of the nerves at relatively low stimulation thresholds of only 50 mW at 1870 nm.

- An alternative diode laser wavelength ($\lambda$ = 1455 nm) was used for optical stimulation of the cavernous nerves which is more compact and less expensive than the Thulium fiber laser ($\lambda$ = 1870 nm) used in previous studies. This laser wavelength was also more efficiently absorbed by the nerves, resulting in an even lower stimulation threshold of only about 30 mW.

- An all-single-mode optical fiber based optical nerve stimulation system was built and tested using the 1455 nm diode laser, and Gaussian and flat-top spatial beam profiles were compared for fast stimulation of the prostate nerves. The stimulation time was further reduced from 30-60 s in Year 1 studies to approximately 9 s in Year 2 studies, now to about 3-4 s using this system.

# REPORTABLE OUTCOMES

**Peer-Reviewed Manuscripts**

Chitchian S, Weldon TP, Fiddy MA, Fried NM. Combined image processing algorithms for improved optical coherence tomography of the prostate nerves. Journal of Biomedical Optics 15(4):046014, 2010.

Tozburun S, Cilip CM, Lagoda GA, Burnett AL, Fried NM. Continuous-wave infrared optical nerve stimulation for potential diagnostic applications. Journal of Biomedical Optics 15(5):055012, 2010.

**Peer-Reviewed Conference Proceedings**

Tozburun S, Cilip CM, Lagoda GA, Burnett AL, Fried NM. Continuous-wave optical stimulation of the rat prostate nerves using an all-single-mode 1455 nm diode laser and fiber system. Proc. SPIE 7883:788352:1-6, 2011.

Chitchian S, Lagoda GA, Burnett AL, Fried NM. Fourier-domain versus time-domain optical coherence tomography of the prostate nerves. Proc. SPIE 7883:788314:1-7, 2011.

Tozburun S, Lagoda GA, Burnett AL, Fried NM. Continuous-wave versus pulsed infrared laser stimulation of the rat prostate cavernous nerves. Proc. SPIE 7883:78831A:1-6, 2011.

# CONCLUSION

In the third year of this project, we completed several studies. First, two different OCT systems (time-domain and Fourier-domain) were compared using several image metrics, including signal-to-noise (SNR), contrast-to-noise (CNR), and equivalent number of looks (ENL). Although the TD-OCT system had a slower image acquisition time, it was found to have superior SNR for deeper imaging of the prostate gland. Second, a continuous-wave (CW) method of optically stimulating the prostate nerves was developed, resulting in faster stimulation of the nerves at relatively low stimulation thresholds of only 50 mW. Third, an alternative diode laser wavelength ($\lambda$ = 1455 nm) was used for optical stimulation of the cavernous nerves which is more compact and less expensive than the Thulium fiber laser ($\lambda$ = 1870 nm) used in previous studies. This laser wavelength was also more efficiently absorbed by the nerves, resulting in a lower stimulation threshold of only approximately 30 mW. Finally, an all-single-mode optical fiber based optical nerve stimulation system was built and tested using the 1455 nm diode laser, and Gaussian and flat-top spatial beam profiles were compared for fast stimulation of the prostate nerves. The stimulation time was further reduced from 30-60 s in Year 1 studies to 9 s in Year 2 studies, to about 3-4 s in the Year 3 studies. Overall, during Year 3 of the grant, we published 2 manuscripts and 3 conference proceedings. Our research results were also presented at the International Symposium for Biomedical Optics (SPIE). In year 4 of the grant, we plan to complete some of the Year 3 tasks associated with rapid, precise, and hemostatic dissection of the prostate from the cavernous nerves using a KTP laser.

# REFERENCES


1. G. P. Murphy, C. Mettlin, H. Menck, D. P. Winchester, and A. M. Davidson, "National patterns of prostate cancer treatment by radical prostatectomy: results of a survey by the American College of Surgeons Committee on Cancer," *J. Urol.*, vol. 152, 1817-1819, 1994.
2. J. A. Talcott, P. Rieker, K. J. Propert, J. A. Clark, K. I. Wishnow, K. R. Loughlin, J. P. Richie, and P. W. Kantoff, "Patient-reported impotence and incontinence after nerve-sparing radical prostatectomy," *J. Natl. Cancer Inst.*, vol. 89, pp. 1117-1123, 1997.
3. V. E. Weldon, F. R. Tavel, and H. Neuwirth, Continence, potency and morbidity after radical perineal prostatectomy," *J. Urol.*, vol. 158:1470-1475, 1997.
4. W. J. Catalona, G. F. Carvalhal, D. E. Mager, and D. S. Smith, "Potency, continence and complication rates in 1,870 consecutive radical retropubic prostatectomies," *J. Urol.*, vol. 162, pp. 433-438, 1999.
5. P. C. Walsh, P. Marschke, D. Ricker, and A. L. Burnett, "Patient-reported urinary continence and sexual function after anatomic radical prostatectomy," *Urol.*, vol. 55, pp. 58-61, 2000.
6. A. L. Burnett, G. Aus, E. D. Canby-Hagino, M. S. Cookson, A. V. D'Amico, R. R. Dmochowski, D. T. Eton, J. D. Forman, S. L. Goldenberg, J. Hernandez, C. S. Higano, S. Kraus, M. Liebert, J. W. Moul, C. Tangen, J. B. Thrasher, I. Thompson, "Erectile function outcome reporting after clinically localized prostate cancer treatment," *J. Urol.*, vol. 178(2), pp. 597-601, 2007.
7. A. J. Costello, M. Brooks, and O. J. Cole, "Anatomical studies of the neurovascular bundle and cavernosal nerves," *BJU Int.*, vol. 94, pp. 1071-1076, 2004.
8. N. M. Fried, S. Rais-Bahrami, G. A. Lagoda, Y. Chuang, A. L. Burnett, and L. M. Su, "Imaging the cavernous nerves in the rat prostate using optical coherence tomography," *Lasers Surg. Med.*, vol. 39, pp. 36-41, 2007.
9. D. Huang, E. A. Swanson, C. P. Lin, J. S. Schuman, W. G. Stinson, W. Chang, M. R. Hee, T. Flotte, K. Gregory, C. A. Puliafito, and J. G. Fujimoto, "Optical coherence tomography," *Science*, vol. 254, pp. 1178-1181, 1991.
10. G. J. Tearney, M. E. Brezinski, B. E. Bouma, S. A. Boppart, C. Pitris, J. F. Southern, and J. G. Fujimoto, "In vivo endoscopic optical biopsy with optical coherence tomography," *Science*, vol. 276, pp. 2037-2039, 1997.
11. F. Koenig, G. J. Tearney, and B. E. Bouma, "Optical coherence tomography in urology," Ch. 28, In Handbook of Optical Coherence Tomography, Eds. B. E. Bouma and G. J. Tearney, Marcel Dekker: New York, 2002.
12. P. Crow, N. Stone, C. A. Kendall, R. A. Persad, and M. P. Wright, "Optical diagnostics in urology: current applications and future prospects," *BJU Int.*, vol. 92, pp. 400-407, 2003.
13. G. J. Tearney, M. E. Brezinski, J. F. Southern, B. E. Bouma, S. A. Boppart, and J. G. Fujimoto, "Optical biopsy in human urologic tissue using optical coherence tomography," *J. Urol.*, vol. 157, pp. 1915-1919, 1997.
14. A. V. D'Amico, M. Weinstein, X. Li, J. P. Richie, and J. Fujimoto, "Optical coherence tomography as a method for identifying benign and malignant microscopic structures in the prostate gland," *Urol.*, vol. 55, pp. 783-787, 2000.
15. S. A. Boppart, J. M. Herrmann, C. Pitris, D. L. Stamper, M. E. Brezinski, and J. G. Fujimoto, "Real-time optical coherence tomography for minimally invasive imaging of prostate ablation," *Comput. Aided Surg.*, vol. 6, pp. 94-103, 2001.
16. L. Klotz, "Neurostimulation during radical prostatectomy: improving nerve-sparing techniques," *Semin. Urol. Oncol.*, vol. 18, pp. 46-50, 2000.
17. H. L. Kim, D. S. Stoffel, D. A. Mhoon, and C. B. Brendler, "A positive caver map response poorly predicts recovery of potency after radical prostatectomy," *Urol.*, vol. 56, pp. 561-564, 2000.

18. L. Klotz, J. Heaton, M. Jewett, J. Chin, N. Fleshner, L. Goldenberg, and M. Gleave, "A randomized phase 3 study of intraoperative cavernous nerve stimulation with penile tumescence monitoring to improve nerve sparing during radical prostatectomy," *J. Urol.*, vol. 164, pp. 1573-1578, 2000.
19. J. Holzbeierlein, M. Peterson, and J. A. Smith Jr, "Variability of results of cavernous nerve stimulation during radical prostatectomy," *J. Urol.*, vol. 165, pp. 108-110, 2001.
20. P. C. Walsh, P. Marschke, W. J. Catalona, H. Lepor, S. Martin, R. P. Myers, and M. S. Steiner, "Efficacy of first-generation Cavermap to verify location and function of cavernous nerves during radical prostatectomy: a multi-institutional study by experienced surgeons," *Urol.*, vol. 57, pp. 491-494, 2001.
21. H. L. Kim, D. A. Mhoon, and C. B. Brendler, "Does the CaverMap device help preserve potency?" *Curr. Urol. Rep.*, vol. 2, pp. 214-217, 2001.
22. L. Klotz, "Cavernosal nerve mapping: current data and applications," *BJU Int.*, vol. 93, pp. 9-13, 2004.
23. J. Wells, C. Kao, K. Mariappan, J. Albea, E. D. Jansen, P. Konrad, and A. Mahadevan-Jansen, "Optical stimulation of neural tissue in vivo," *Opt. Lett.*, vol. 30, pp. 504-506, 2005.
24. J. Wells, C. Kao, E. D. Jansen, P. Konrad, and A. Mahadevan-Jansen, "Application of infrared light for in vivo neural stimulation," *J. Biomed. Opt.*, vol. 10:064003, pp. 1-11, 2005.
25. A. D. Izzo, C. P. Richter, E. D. Jansen, and J. T. Walsh, "Laser stimulation of the auditory nerve," *Lasers Surg. Med.*, vol. 38, pp. 745-753, 2006.
26. A. D. Izzo, J. T. Walsh, E. D. Jansen, M. Bendett, J. Webb, H. Ralph, and C. P. Richter, "Optical parameter variability in laser nerve stimulation: a study of pulse duration, repetition rate, and wavelength," *IEEE Trans. Biomed. Eng.*, vol. 54, pp. 1108-1114, 2007.
27. J. D. Wells, S. Thomsen S, P. Whitaker, E. D. Jansen, C. C. Kao, P. E. Konrad, A. Mahadevan-Jansen, "Optical mediated nerve stimulation: identification of injury thresholds," *Lasers Surg. Med.* vol. 39, pp. 513-526, 2007.
28. J. Bush, P. Davis, and M. A. Marcus, "All-fiber optic coherence domain interferometric techniques," *Proc. SPIE*, vol. 4204A-08, 2000.
29. F. Feldchtein, J. Bush J, G. Gelikonov, V. Gelikonov, and S. Piyevsky S, "Cost-effective, all-fiber autocorrelator based 1300 nm OCT system," *Proc. SPIE*, vol. 5690, pp. 349-354, 2005.
30. U. Sharma, N. M. Fried, and J. U. Kang, "All-fiber common-path optical coherence tomography: sensitivity optimization and system analysis," *IEEE J. Sel. Top. Quant. Electron.*, vol. 11, pp. 799-805, 2005.
31. F. Feldchtein, N. Tresser, M. Kareta, D. Bodner, I. Gill, J. Kaouk, P. Kick, G. MacLennan, W. Kuang, L. Schoenfeld, E. Klein, M. Resnick, "Niris optical coherence tomography system: principle of operation and applications in endourology," *J. Endourol.*, vol. 20 (Suppl 1):A198, 2006.
32. M. Aron, J. H. Kaouk, N. J. Hegarty, J. R. Colombo, Jr., G. P. Haber, B. I. Chung, M. Zhou, I. S. Gill, "Preliminary experience with the Niris optical coherence tomography system during laparoscopic and robotic prostatectomy," *J. Endourol.*, vol. 21(8), pp. 814-818, 2007.

# APPENDIX

**Peer-Reviewed Manuscripts**

Chitchian S, Weldon TP, Fiddy MA, Fried NM. Combined image processing algorithms for improved optical coherence tomography of the prostate nerves. Journal of Biomedical Optics 15(4):046014, 2010.

Tozburun S, Cilip CM, Lagoda GA, Burnett AL, Fried NM. Continuous-wave infrared optical nerve stimulation for potential diagnostic applications. Journal of Biomedical Optics 15(5):055012, 2010.

**Peer-Reviewed Conference Proceedings**

Tozburun S, Cilip CM, Lagoda GA, Burnett AL, Fried NM. Continuous-wave optical stimulation of the rat prostate nerves using an all-single-mode 1455 nm diode laser and fiber system. Proc. SPIE 7883:788352:1-6, 2011.

Chitchian S, Lagoda GA, Burnett AL, Fried NM. Fourier-domain versus time-domain optical coherence tomography of the prostate nerves. Proc. SPIE 7883:788314:1-7, 2011.

Tozburun S, Lagoda GA, Burnett AL, Fried NM. Continuous-wave versus pulsed infrared laser stimulation of the rat prostate cavernous nerves. Proc. SPIE 7883:78831A:1-6, 2011.

# Combined image-processing algorithms for improved optical coherence tomography of prostate nerves

**Shahab Chitchian**
University of North Carolina at Charlotte
Department of Physics and Optical Science
Charlotte, North Carolina 28223

**Thomas P. Weldon**
University of North Carolina at Charlotte
Department of Electrical and Computer Engineering
Charlotte, North Carolina 28223

**Michael A. Fiddy**
University of North Carolina at Charlotte
Department of Physics and Optical Science
Charlotte, North Carolina 28223

**Nathaniel M. Fried**
University of North Carolina at Charlotte
Department of Physics and Optical Science
Charlotte, North Carolina 28223
and
Johns Hopkins Medical Institutions
Department of Urology
Baltimore, Maryland 21287

**Abstract.** Cavernous nerves course along the surface of the prostate gland and are responsible for erectile function. These nerves are at risk of injury during surgical removal of a cancerous prostate gland. In this work, a combination of segmentation, denoising, and edge detection algorithms are applied to time-domain optical coherence tomography (OCT) images of rat prostate to improve identification of cavernous nerves. First, OCT images of the prostate are segmented to differentiate the cavernous nerves from the prostate gland. Then, a locally adaptive denoising algorithm using a dual-tree complex wavelet transform is applied to reduce speckle noise. Finally, edge detection is used to provide deeper imaging of the prostate gland. Combined application of these three algorithms results in improved signal-to-noise ratio, imaging depth, and automatic identification of the cavernous nerves, which may be of direct benefit for use in laparoscopic and robotic nerve-sparing prostate cancer surgery.  [DOI: 10.1117/1.3481144]

Keywords: optical coherence tomography; prostate gland; cavernous nerve; prostate cancer.

Paper 09537RR received Dec. 2, 2009; revised manuscript received May 21, 2010; accepted for publication Jun. 21, 2010; published online Aug. 20, 2010.

## 1 Introduction

Preservation of cavernous nerves during radical prostatectomy for prostate cancer is critical for preserving sexual function after surgery. These nerves are at risk of injury during dissection and removal of a cancerous prostate gland because of the close proximity of the nerves to the prostate surface (Fig. 1). Their microscopic nature also makes it difficult to predict the true course and location of these nerves from one patient to another. These observations may explain in part the wide variability in reported potency rates (9 to 86%) following prostate cancer surgery.[1] Therefore, any technology capable of providing improved identification, imaging, and visualization of the cavernous nerves during prostate cancer surgery would aid the preservation of the nerves and improve postoperative sexual potency.

OCT is a noninvasive optical imaging technique that can be used to perform high-resolution, cross sectional *in vivo* and *in situ* imaging of microstructures in biological tissues.[2] OCT imaging of cavernous nerves in rat and human prostate has recently been demonstrated.[3–6] However, improvements in the quality of the OCT images for identification of the cavernous nerves are necessary before clinical use.

For the present work, OCT images were acquired *in vivo* using a clinical endoscopic OCT system (Imalux, Cleveland, Ohio) based on an all single-mode fiber common-path interferometer-based scanning system (Optiphase, Van Nuys, California). An 8-Fr (2.6-mm-OD) probe was used with the OCT system. The system is capable of acquiring real-time images at $200 \times 200$ pixels with 11-$\mu$m axial and 25-$\mu$m lateral resolutions in tissue.

The following study describes a step-by-step approach that employs three complementary image processing algorithms (Fig. 2) for improving identification and imaging of the cavernous nerves during OCT of the prostate gland. In previous work, a segmentation approach was successfully used to identify the cavernous nerves.[7] However, it has proven challenging to image deeper prostate tissues with OCT. Therefore, the segmentation system in the left branch of Fig. 2 is augmented by the denoising and edge detection systems in the right branch of Fig. 2. This edge detection system is later shown to improve OCT imaging of deeper prostate tissue structures.

In the left branch of Fig. 2, 2-D OCT images of rat prostate are segmented to differentiate the cavernous nerves from the prostate gland. It should be noted that ultrasound image segmentation of the prostate, which allows clinicians to design an accurate brachytherapy treatment plan for prostate cancer, has been previously reported.[8] Various alternative segmentation approaches have also recently been applied in retinal OCT imaging.[9–16] However, large irregular voids in prostate OCT images require a segmentation approach different than that used for segmentation of the more regular structure of retinal layers. Therefore, to detect cavernous nerves, three image features are employed: a Gabor filter, Daubechies wavelet, and Laws filter. The Gabor feature is applied with different stan-

Address all correspondence to: Shahab Chitchian, University of North Carolina at Charlotte, Department of Physics and Optical Science, Charlotte, NC 28223. Tel: 704-687-8152; Fax: 704-687-8197; E-mail: schitchi@uncc.edu

1083-3668/2010/15(4)/046014/6/$25.00 © 2010 SPIE

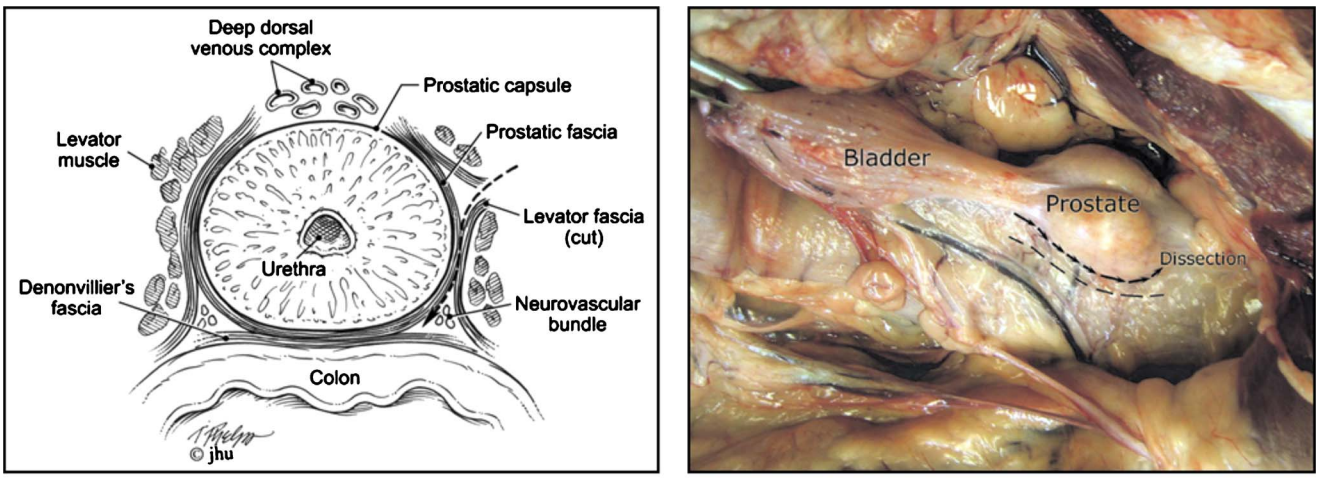


**Fig. 1** (a) Cross sectional diagram of the human prostate showing the location of the neurovascular bundles and their close proximity to the prostate surface. The dotted line indicates the route of dissection between the prostatic capsule and the neurovascular bundle. (b) Image of human prostate during surgery. Arrows indicate the surgical dissection plane, and the dashed line indicates the position of the periprostatic neurovascular bundle under a superficial layer of fascia.

dard deviations in the $x$ and $y$ directions. In the Daubechies wavelet feature, an eight-tap Daubechies orthonormal wavelet is implemented, and the low-pass subband is chosen as the filtered image. Finally, Laws feature extraction is applied to the images. The features are segmented using a nearest-neighbor classifier. N-ary morphological postprocessing is used to remove small voids.

As a next step to improve OCT imaging of the prostate gland, wavelet denoising is applied. Recently, wavelet techniques have been employed successfully in speckle noise reduction for MRI, ultrasound, and OCT images.[17–19] A locally adaptive denoising algorithm is applied before edge detection to reduce speckle noise in OCT images of the prostate.[20] The denoising algorithm is illustrated using the dual-tree complex wavelet transform. After wavelet denoising, an edge detection algorithm based on thresholding and spatial first-order differentiation is implemented to provide deeper imaging of the prostate gland. This algorithm addresses one of the main limitations in OCT imaging of the prostate tissue, which is the inability to image deep into the prostate. Currently, OCT is limited to an image depth of approximately 1 mm in most opaque soft tissues. In the following sections, a segmentation approach is first described, followed by details of denoising and edge detection approaches.

## 2 Segmentation System

The input image is first processed to form three feature images. The prostate image is then segmented into nerve, prostate, and background classes using a $k$-nearest neighbors classifier and the three feature images. Finally, N-ary morphology is used for postprocessing. The generation of the feature images are first described, followed by descriptions of the classifier and postprocessing.

### 2.1 *Gabor Filter*

The first feature image is generated by a Gabor filter with impulse response $h(x,y)$,[21]

$$h(x,y) = g(x,y)\exp[j2\pi(Ux + Vy)], \tag{1}$$

where

$$g(x,y) = \frac{1}{2\pi\sigma_x\sigma_y}\exp\left[-\frac{1}{2}\left(\frac{x^2}{\sigma_x^2} + \frac{y^2}{\sigma_y^2}\right)\right]. \tag{2}$$

The Gabor function is essentially a bandpass filter centered about frequency $(U,V)$ with bandwidth determined by $\sigma_x, \sigma_y$. The Gabor feature center frequency of $(0.2, 0.2)$ cycles/pixel is applied with standard deviations of 3 and 6 in the $x$ and $y$ directions, respectively, based on experimental observation of minimum segmentation error.

### 2.2 *Daubechies Wavelet Transform*

The second feature is generated by the eight-tap Daubechies orthonormal wavelet transform. The discrete wavelet transform (DWT) converts a signal to its wavelet representation. In a one-level DWT, the image $c_0$ is split into an approximation

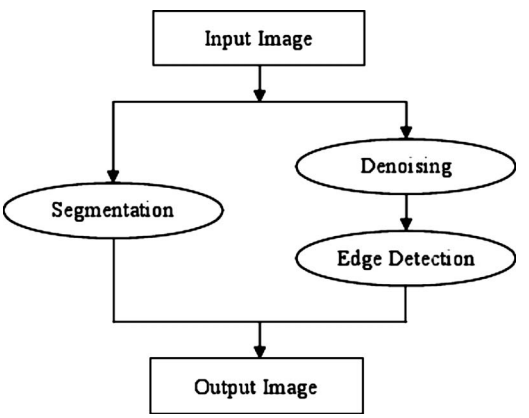


**Fig. 2** Flow chart describing a step-by-step application of complementary image processing algorithms for OCT of the prostate nerves.

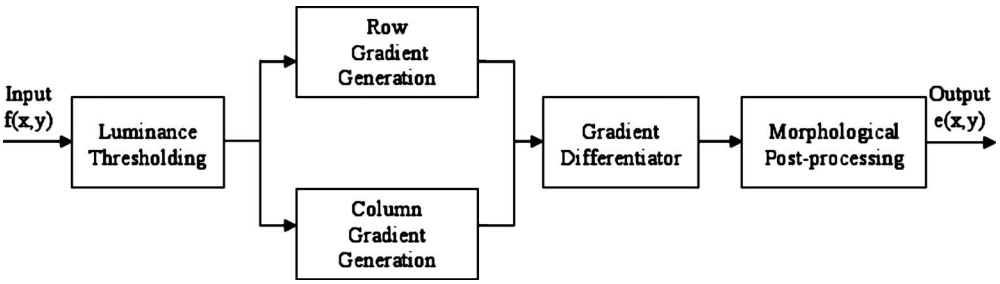


**Fig. 3** Edge detection system block diagram.

part $c_1$ and detail parts $d_1^1$, $d_1^2$, and $d_1^3$ for horizontal, vertical, and diagonal orientations, respectively. In a multilevel DWT, each subsequent $c_i$ is split into an approximation $c_{i+1}$ and details $d_{i+1}^1$, $d_{i+1}^2$, and $d_{i+1}^3$. In the present work, the approximation part $c_1$ is chosen as the filtered image for the second feature.

### 2.3 *Laws Filter*

The third feature is generated by the Laws feature extraction method. Laws 2 mask $h(x,y)$[22] is convolved with the image to accentuate its microstructure. The microstructure image $m(x,y)$ is defined as

$$m(x,y) = f(x,y) * h(x,y), \tag{3}$$

where

$$\mathbf{h} = \frac{1}{12}\begin{pmatrix} 1 & 0 & -1 \\ 2 & 0 & -2 \\ 1 & 0 & -1 \end{pmatrix}. \tag{4}$$

Then, standard deviation computation is performed after the Laws mask filtering to complete the Laws feature extraction.

### 2.4 *K-Nearest Neighbor Classifier and Postprocessing*

The *k*-nearest neighbors algorithm (*k*-NN) is a method for classifying objects where classification is based on the *k* closest training samples in the feature space. It is implemented by training, parameter selection, and classification steps, followed by the N-ary morphological postprocessing method for eliminating small misclassified regions.[7]

## 3 Wavelet Shrinkage Denoising

Wavelet shrinkage is denoising by shrinking (nonlinear soft thresholding) in the wavelet transform domain. The observed image $X$ is modeled as an uncorrupted image $S$ and multiplicative speckle noise $N$. On a logarithmic scale, speckle is converted to additive noise $X=S+N$. The wavelet shrinkage denoising algorithm requires the following four-step procedure,[20]

$$Y = W(X), \quad \lambda = d(Y), \quad Z = D(Y,\lambda), \quad S = W^{-1}(Z), \tag{5}$$

where operator $W(.)$ relates to the wavelet transform, operator $d(.)$ selects a data-adaptive threshold, $D(.,\lambda)$ denotes the denoising operator with threshold $\lambda$, and $W^{-1}$ relates the inverse wavelet transform.

### 3.1 *Two-Dimensional Dual-Tree Complex Wavelet Transform*

In the proposed method, the dual-tree complex wavelet transform (CDWT) calculates the complex transform of a signal using two separate DWT decompositions. If the filters used in one are specifically designed differently from those in the other, it is possible for one DWT to produce the real coefficients and the other the imaginary coefficients. This redundancy of two provides extra information for analysis at the expense of extra computational power.

In the proposed CDWT, wavelet coefficients are calculated from the Farras nearly symmetric wavelet.[23]

### 3.2 *Shrinkage Denoising*

Bivariate shrinkage with a local variance estimation algorithm[24] is applied for shrinkage denoising. After estimating the signal components of the noisy coefficients in the wavelet domain, the inverse wavelet transform is taken to reconstruct the noise-free image.

## 4 Edge Detection System

A block diagram of the edge detection system is shown in Fig. 3. After luminance thresholding on the input image $f(x,y)$, a first-order spatial differentiator of orthogonal gradient is performed to produce the differential image $g(x,y)$ with accentuated spatial amplitude changes. Morphological postprocessing is then used to accentuate edges.

### 4.1 *Luminance Thresholding*

In this section, the glandular structure of the prostate is judged present if the luminance exceeds the threshold level of the background. The center of the glandular structures, below the boundary, in the denoised prostate image represents the background threshold level, because the boundaries of these glandular structures can be located at a superficial level.

### 4.2 *Orthogonal Gradient Generation*

After applying the threshold level to the denoised image $f(x,y)$, a form of spatial first-order differentiation is performed in two orthogonal directions. In the discrete domain, the gradient in each direction is generated by[22]

$$g_{r,c}(x,y) = f(x,y) * h_{r,c}(x,y), \tag{6}$$

where

$$\mathbf{h}_r = \frac{1}{4}\begin{pmatrix} 1 & 0 & -1 \\ 2 & 0 & -2 \\ 1 & 0 & -1 \end{pmatrix}, \quad \mathbf{h}_c = \frac{1}{4}\begin{pmatrix} -1 & -2 & -1 \\ 0 & 0 & 0 \\ 1 & 2 & 1 \end{pmatrix}, \qquad (7)$$

are the row and column impulse response arrays for the $3 \times 3$ Sobel orthogonal gradient operator.

The gradient amplitude is approximated by the magnitude combination

$$g(x,y) = |g_r(x,y)| + |g_c(x,y)|. \qquad (8)$$

### 4.3 *Morphological Postprocessing*

Morphological postprocessing for accentuating edges proceeds by close operation. It is implemented by dilation followed by erosion.

## 5 Combined Algorithms

Figure 2 shows the order of the combined algorithms. The segmentation algorithm was applied to differentiate the cavernous nerves from the prostate gland. This algorithm is independent of the denoising process. However, the edge detection algorithm to provide deeper imaging of the prostate gland based on thresholding and spatial first-order differentiation is dependent on the denoising process. In other words, edges are sensitive to the noise. First, the input image was denoised, then the edge detection was implemented. With a noisy image, threshold selection becomes a tradeoff between missing valid edges and creating noise-induced false edges.

The algorithms were executed on a Core 2 Duo, 1.86-GHz desktop personal computer. There were two parallel processes of Fig. 2, 8-s denoising and edge detection and 10-s segmentation. The total time for the combined processing algorithms was 10 s.

## 6 Results

The unprocessed time-domain (TD)-OCT images of the cavernous nerves at different orientations (longitudinal, oblique, and cross sectional) along the surface of the rat prostate are shown in Figs. 4(a), 4(c), and 4(e). Histologic sections of the cavernous nerves were previously processed for comparison.[20]

Figures 4(b), 4(d), and 4(f) show the images after denoising using CDWT. The global signal-to-noise ratio (SNR) is calculated as

$$\mathrm{SNR} = 10 \times \log[\max(X_{\mathrm{lin}})^2/\sigma_{\mathrm{lin}}^2], \qquad (9)$$

where $X_{\mathrm{lin}}$ is the 2-D matrix of pixel values in the OCT image and $\sigma_{\mathrm{lin}}^2$ is the noise variance, both on linear intensity scales.[25] The mean value of SNR for nine sample images before and after denoising was measured to be 26.65 and 40.87, respectively. Therefore, a SNR increase of approximately 14 dB was attained.

Figures 5(a), 5(c), and 5(e) show the same OCT images of Figs. 4(a), 4(c), and 4(e) after segmentation. The cavernous nerves could be differentiated from the prostate gland using the segmentation algorithm. The error rate was calculated by: error=(number of error pixels)/(number of total pixels), where (number of error pixels)=(number of false positives +number of false negatives). The overall error rate for the segmentation of the nerves was 0.058 with a standard deviation of 0.019, indicating the robustness of our technique. The error rate was measured as a mean of error measurements for three different sample images at different orientations (longitudinal, cross sectional, and oblique). A different image was used for training. The error rate was determined by comparing manually segmented images to the automatically segmented images of the nerves. These manually segmented images of the cavernous nerves were previously created according to histologic correlation with OCT images.[20] Figures 5(b), 5(d), and 5(f) combine edge detection of the denoised images and the segmentation results. Manual segmentation of the prostate gland was implemented to calculate performance of the edge detection algorithm. The overall error rate for the segmentation of the prostate gland was 0.076 with a standard deviation of 0.022.

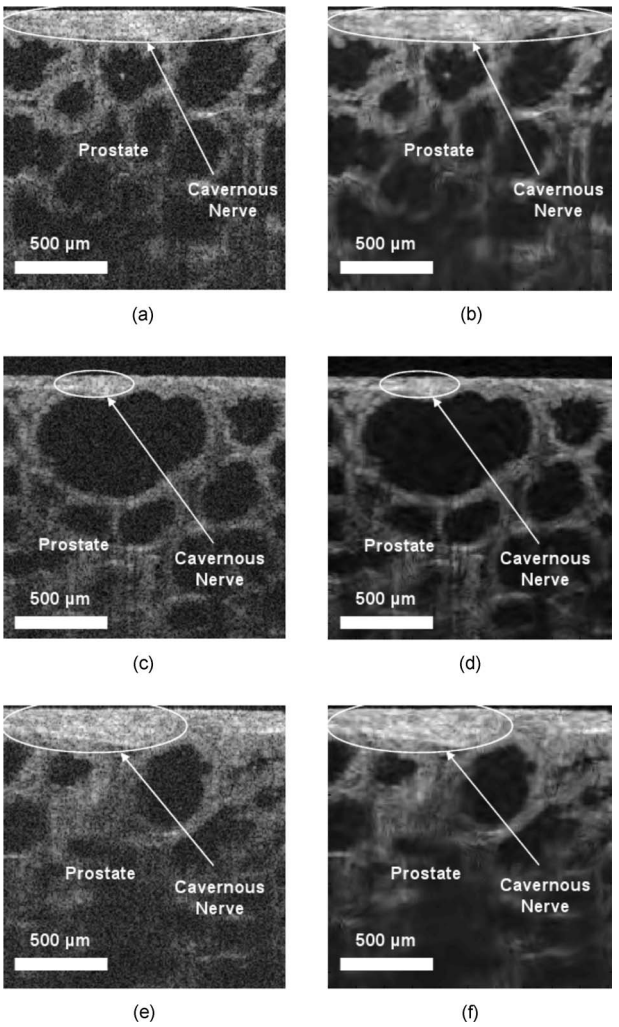


**Fig. 4** OCT images of the rat cavernous nerve: (a) and (b) longitudinal section; (c) and (d) cross section; (e) and (f) oblique section. (a), (c), and (e) show before; and (b), (d), and (f) show after denoising.

## 7 Discussion

The proposed edge detection approach was successful in accentuating prostate structures deeper in the tissue, and the

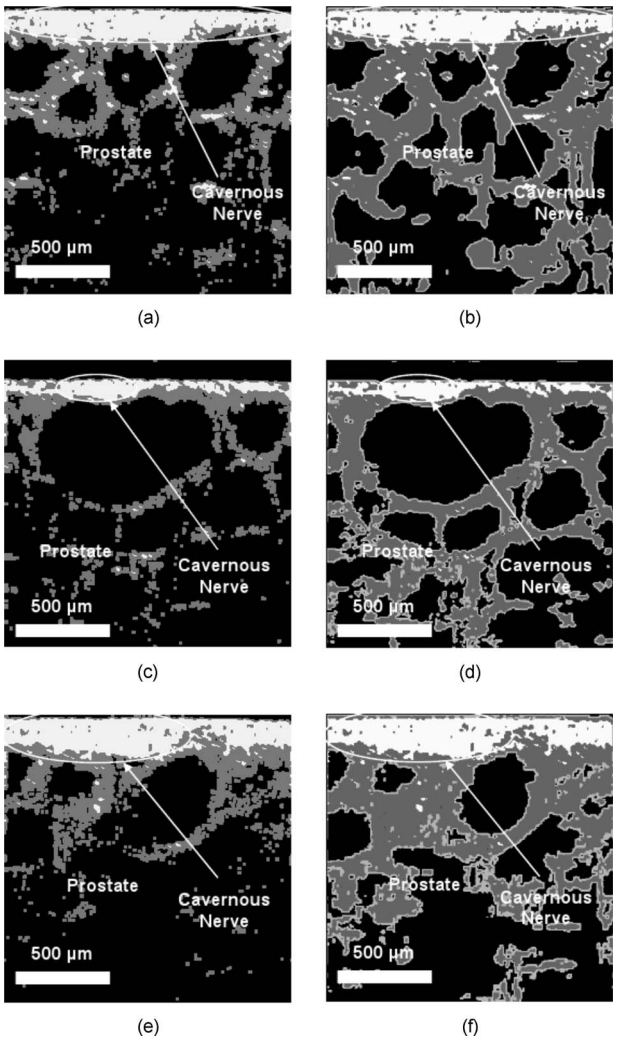


**Fig. 5** OCT images of the rat cavernous nerve: (a) and (b) longitudinal section; (c) and (d) cross section; (e) and (f) oblique section. (a), (c), and (e) show segmented and (b), (d), and (f) show edge detected images.

cavernous nerves could be differentiated from the prostate gland using the segmentation algorithm. The glandular structure of the prostate could be observed to a depth of approximately 1.6 mm in Figs. 5(b), 5(d), and 5(f) in comparison with an approximately 1-mm depth in the unprocessed OCT images in Figs. 4(a), 4(c), and 4(e). Overall, the edge detection technique enhanced structures deeper in the prostate gland, and the proposed image segmentation algorithm performed well for identification of the cavernous nerves in the prostate.

It should also be noted that the rat model used in this study represents an idealized version of the prostate anatomy, because the cavernous nerve lies on the surface of the prostate, and is therefore directly visible. However, in human anatomy, there can be an intervening layer of fascia (Fig. 1) between the OCT probe and the nerves, making identification more difficult. Since one major limitation of OCT is its superficial imaging depth in opaque tissues, an important advantage of these image processing algorithms is that the final OCT image should be able to provide deeper imaging in the tissue and locate the cavernous nerve when it lies at various depths beneath periprostatic tissues.

## 8 Conclusion

The segmentation technique is applied to differentiate cavernous nerves from the prostate gland in rat prostate. The wavelet shrinkage denoising technique using a dual-tree complex wavelet transform is used for speckle noise reduction, and by using edge detection, deeper imaging of the prostate gland is accomplished. These algorithms for image segmentation, denoising, and edge detection of the prostate may be of direct benefit for implementation in clinical endoscopic OCT systems currently being studied for use in laparoscopic and robotic nerve-sparing prostate cancer surgery.

### *Acknowledgments*

This research was supported in part by the Department of Defense Prostate Cancer Research Program, grant number PC073709, and the Department of Energy, grant number DE-FG02-06CH11460. The authors thank Paul Amazeen and Nancy Tresser of Imalux Corporation (Cleveland, Ohio) for providing the OCT system used in these studies.

### *References*

1. A. Burnett, G. Aus, E. Canby-Hagino, M. Cookson, A. D'Amico, R. Dmochowski, D. Eton, J. Forman, S. Goldenberg, J. Hernandez, C. Higano, S. Kraus, M. Liebert, J. Moul, C. Tangen, J. Thrasher, and I. Thompson, "Function outcome reporting after clinically localized prostate cancer treatment," *J. Urol.* **178**, 597–601 (2007).
2. D. Huang, E. Swanson, C. Lin, J. Schuman, W. Stinson, W. Chang, M. Hee, T. Flotte, K. Gregory, C. Puliafito, and J. Fujimoto, "Optical coherence tomography," *Science* **254**, 1178–1181 (1991).
3. M. Aron, J. Kaouk, N. Hegarty, J. Colombo, G. Haber, B. Chung, M. Zhou, and I. Gill, "Preliminary experience with the niris optical coherence tomography system during laparoscopic and robotic prostatectomy," *J. Endourol* **21**, 814–818 (2007).
4. N. Fried, S. Rais-Bahrami, G. Lagoda, A. Chuang, A. Burnett, and L. Su, "Imaging the cavernous nerves in rat prostate using optical coherence tomography," *Lasers Surg. Med.* **39**, 36–41 (2007).
5. N. M. Fried, S. Rais-Bahrami, G. A. Lagoda, A.-Y. Chuang, L.-M. Su, and A. L. Burnett, "Identification and imaging of the nerves responsible for erectile function in rat prostate, *in vivo*, using optical nerve stimulation and optical coherence tomography," *IEEE J. Sel. Top. Quantum Electron.* **13**, 1641–1645 (2007).
6. S. Rais-Bahrami, A. W. Levinson, N. M. Fried, G. A. Lagoda, A. Hristov, Y. Chuang, A. L. Burnett, and L.-M. Su, "Optical coherence tomography of cavernous nerves: A step toward real-time intraoperative imaging during nerve-sparing radical prostatectomy," *Urology* **72**, 198–204 (2008).
7. S. Chitchian, T. Weldon, and N. Fried, "Segmentation of optical coherence tomography images for differentiation of the cavernous nerves from the prostate gland," *J. Biomed. Opt.* **14**(4), 044033 (2009).
8. J. Noble and D. Boukerroui, "Ultrasound image segmentation: a survey," *IEEE Trans. Med. Imaging* **25**, 987–1010 (2006).
9. D. Cabrera Fernández, H. M. Salinas, and C. A. Puliafito, "Automated detection of retinal layer structures on optical coherence tomography images," *Opt. Express* **13**, 10200–10216 (2005).
10. M. Szkulmowski, M. Wojtkowski, B. Sikorski, T. Bajraszewski, V. Srinivasan, A. Szkulmowska, J. Kaluzny, J. Fujimoto, and A. Kowalczyk, "Analysis of posterior retinal layers in spectral optical coherence tomography images of the normal retina and retinal pathologies," *J. Biomed. Opt.* **12**(4), 041207 (2007).
11. M. Haeker, M. Sonka, R. Kardon, V. Shah, X. Wu, and M. Abramoff, "Automated segmentation of intraretinal layers from macular optical coherence tomography images," *Proc. SPIE* **6512**, 651214 (2007).
12. M. Garvin, M. Abramoff, R. Kardon, S. Russell, X. Wu, and M. Sonka, "Intraretinal layer segmentation of macular optical coherence

tomography images using optimal 3-D graph search," *IEEE Trans. Med. Imaging* **27**, 1495–1505 (2008).
13. E. Gotzinger, M. Pircher, W. Geitzenauer, C. Ahlers, B. Baumann, S. Michels, U. Schmidt-Erfurth, and C. Hitzenberger, "Retinal pigment epithelium segmentation by polarization sensitive optical coherence tomography," *Opt. Express* **16**, 16410–16422 (2008).
14. C. Ahlers, C. Simader, W. Geitzenauer, G. Stock, P. Stetson, S. Dastmalchi, and U. Schmidt-Erfurth, "Automatic segmentation in three-dimensional analysis of fibrovascular pigmentepithelial detachment using high-definition optical coherence tomography," *Br. J. Ophthamol.* **92**, 197–203 (2008).
15. T. Fabritius, S. Makita, M. Miura, R. Myllyla, and Y. Yasuno, "Automated segmentation of the macula by optical coherence tomography," *Opt. Express* **17**, 15659–15669 (2009).
16. A. Mishra, A. Wong, K. Bizheva, and D. Clausi, "Intra-retinal layer segmentation in optical coherence tomography images," *Opt. Express* **17**, 23719–23728 (2009).
17. D. Adler, T. Ko, and J. Fujimoto, "Speckle reduction in optical coherence tomography images by use of a spatially adaptive wavelet filter," *Opt. Lett.* **29**, 2878–2880 (2004).
18. A. Pizurica, A. Wink, E. Vansteenkiste, W. Philips, and J. Roerdink, "A review of wavelet denoising in MRI and ultrasound brain imaging," *Curr. Med. Imag. Rev.* **2**, 247–260 (2006).
19. A. Pizurica, L. Jovanov, B. Huysmans, V. Zlokolica, P. Keyser, F. Dhaenens, and W. Philips, "Multiresolution denoising for optical coherence tomography: a review and evaluation," *Curr. Med. Imag. Rev.* **4**, 270–284 (2008).
20. S. Chitchian, M. Fiddy, and N. Fried, "Denoising during optical coherence tomography of the prostate nerves via wavelet shrinkage using dual-tree complex wavelet transform," *J. Biomed. Opt.* **14**(1), 014031 (2009).
21. T. Weldon, W. Higgins, and D. Dunn, "Efficient Gabor filter design for texture segmentation," *Pattern Recogn.* **29**, 2005–2015 (1996).
22. W. Pratt, *Digital Image Processing*, Wiley, New York (2007).
23. A. Abdelnour and I. Selesnick, "Design of 2-band orthogonal near-symmetric CQF," in *Proc. IEEE Intl. Conf. Acoust. Speech, Sign. Process. (ICASSP)*, pp. 3693 (2001).
24. L. Sendur and I. Selesnick, "Bivariate shrinkage with local variance estimation," *IEEE Signal Process. Lett.* **9**, 438–441 (2002).
25. S. Xiang, L. Zhou, and J. Schmitt, "Speckle noise reduction for optical coherence tomography," *Proc. SPIE* **3196**, 79–88 (1998).

# Continuous-wave infrared optical nerve stimulation for potential diagnostic applications

**Serhat Tozburun**
**Christopher M. Cilip**
University of North Carolina at Charlotte
Department of Physics and Optical Science
North Carolina

**Gwen A. Lagoda**
**Arthur L. Burnett**
Johns Hopkins Medical Institutions
Department of Urology
Baltimore, Maryland

**Nathaniel M. Fried**
University of North Carolina at Charlotte
Department of Physics and Optical Science
North Carolina
and
Johns Hopkins Medical Institutions
Department of Urology
Baltimore, Maryland

**Abstract.** Optical nerve stimulation using infrared laser radiation has recently been developed as a potential alternative to electrical nerve stimulation. However, recent studies have focused primarily on pulsed delivery of the laser radiation and at relatively low pulse rates. The objective of this study is to demonstrate faster optical stimulation of the prostate cavernous nerves using continuous-wave (cw) infrared laser radiation for potential diagnostic applications. A thulium fiber laser ($\lambda = 1870$ nm) is used for noncontact optical stimulation of the rat prostate cavernous nerves *in vivo*. Optical nerve stimulation, as measured by an intracavernous pressure (ICP) response in the penis, is achieved with the laser operating in either cw mode, or with a 5-ms pulse duration at 10, 20, 30, 40, 50, and 100 Hz. Successful optical stimulation is observed to be primarily dependent on a threshold nerve temperature (42 to 45 °C), rather than an incident fluence, as previously reported. cw optical nerve stimulation provides a significantly faster ICP response time using a lower power (and also less expensive) laser than pulsed stimulation. cw optical nerve stimulation may therefore represent an alternative mode of stimulation for intraoperative diagnostic applications where a rapid response is critical, such as identification of the cavernous nerves during prostate cancer surgery. 
[DOI: 10.1117/1.3500656]

Keywords: cavernous; laser; nerve; optical; prostate; stimulation; thulium.

Paper 10337LRR received Jun. 16, 2010; revised manuscript received Sep. 13, 2010; accepted for publication Sep. 15, 2010; published online Oct. 12, 2010.

## 1 Introduction

Conventional electrical nerve stimulation (ENS) has several general limitations, as previously reported.[1] First, ENS is limited by the need for physical contact between the electrode and the tissue, which can result in tissue damage. Second, the spatial precision of ENS is limited by the electrode's size. Third, ENS produces artifacts that can interfere with measurement.

Recently, Wells et al. developed optical nerve stimulation (ONS) using pulsed infrared laser radiation[1] as a potential alternative to ENS. They determined that ONS offered several advantages over ENS, including: 1. a noncontact method of stimulation, 2. improved spatial selectivity, and 3. elimination of stimulation artifacts.

For our specific clinical application of interest, intraoperative electrical nerve mapping devices have been tested as surgical diagnostic tools to assist in identification and preservation of the cavernous nerves (CN) and erectile function during nerve-sparing prostate cancer surgery.[2] However, these nerve mapping technologies have proven inconsistent and unreliable in identifying the CN and evaluating nerve function.[3]

Therefore, our laboratory has recently begun studying ONS as an alternative to ENS in a rat cavernous nerve model *in vivo*.[4–6] During initial studies, we focused primarily on the role of laser wavelength, pulse energy, and spatial beam profile on ONS, with less attention spent on the effect of the operation mode (e.g., cw versus pulsed).

Recent studies by other research groups using infrared laser radiation for ONS have also focused primarily on the use of laser radiation delivered in pulsed mode and at relatively low pulse repetition rates (2 to 13 Hz), presumably to avoid thermal build-up and thermal damage to the nerves during long-term stimulation applications.[1,7–9] However, our research group is instead interested in the potential of ONS to be used as an intraoperative diagnostic tool, specifically for identification and preservation of the cavernous nerves during laparoscopic and robotic prostate cancer surgery. Practical application of ONS would thus require rapid short-term nerve stimulation for identification of the cavernous nerves. Therefore, for this current study, we chose to explore delivery of infrared laser radiation to the nerve at significantly higher pulse rates (10 to 100 Hz) and in cw mode, with the hypothesis that this method may result in a more rapid response for identification of the cavernous nerves.

Address all correspondence to: Nathaniel Fried, Department of Physics and Optical Science, University of North Carolina at Charlotte, 9201 University City Avenue, Charlotte, NC 28223-0001. Tel: 704-687-8149; Fax: 704-687-8197; E-mail: nmfried@uncc.edu

1083-3668/2010/15(5)/055012/4/$25.00 © 2010 SPIE

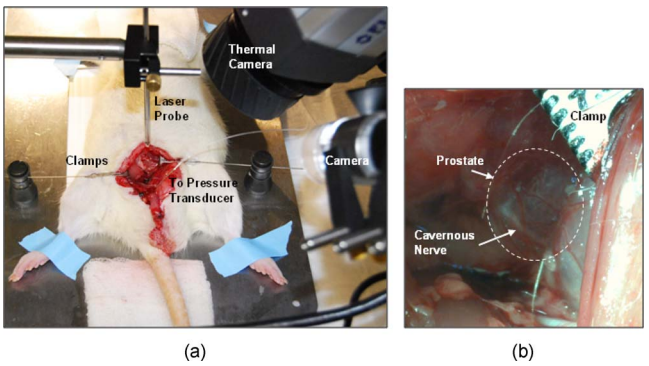


**Fig. 1** Experimental setup for optical stimulation of the rat cavernous nerves: (a) complete setup, and (b) close-up view of the cavernous nerve on the surface of prostate.

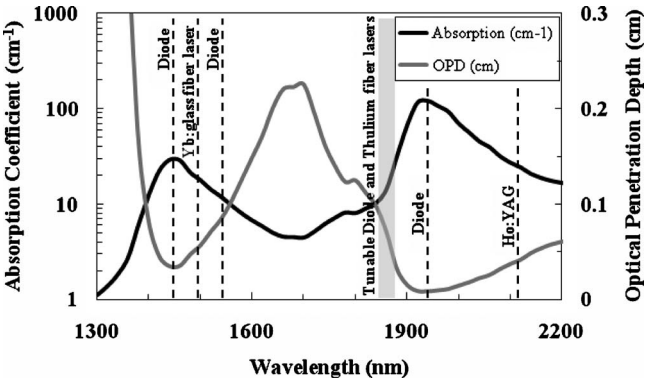


**Fig. 2** Plot of the absorption coefficient and optical penetration depth in water as a function of laser wavelength. Water is the primary chromophore for soft tissues in the near-infrared spectrum. The wavelengths of some relevant lasers for optical nerve stimulation are also labeled.

## 2 Methods

Seven Sprague Dawley rats (400 to 600 g) were anesthetized by intraperitoneal injection with 50-mg/kg sodium pentobarbital. The rats were secured in the supine position and prepped for surgery. The cavernous nerve (CN) arising from the ipsilateral major pelvic ganglion situated dorsolateral to the prostate was exposed via a midline suprapubic incision and anterior pelvic dissection (Fig. 1). To assess intracavernous pressure (ICP), the shaft of the penis was denuded of skin and the left crural region was cannulated with a 23-G needle connected via polyethylene tubing to a pressure transducer (Harvard Apparatus, Holliston, Massachusetts). An increase in ICP after optical stimulation of the CN was detected by a data acquisition system (DI-190, Dataq Instruments, Akron, Ohio). The response parameters were analyzed with MatLab software (Mathworks, Natick, Massachusetts). The ONS experiments were performed under an approved animal protocol, and at the completion of the study the rats were euthanized by intracardiac injection of potassium chloride while under anesthesia, as is consistent with the recommendations of the Panel of Euthanasia of the American Veterinary Medical Association.

Optical nerve stimulation was performed with a thulium fiber laser (TLT-5, IPG Photonics, Oxford, Massachusetts) using a similar wavelength ($\lambda = 1870$ nm) and pulse duration (5 ms) as previously reported.[6] The 1870-nm laser wavelength was chosen because it corresponds to an optical penetration depth in water, the primary chromophore in soft tissues, of approximately 400 $\mu$m (Fig. 2),[10] which closely matches the cavernous nerve diameter, for uniform irradiation and stimulation. (An optical penetration depth significantly less than the nerve diameter would increase the probability of thermal damage to the nerve, and an optical penetration depth significantly greater than the nerve diameter would be less efficient for ONS.) A laser pulse duration of 5 ms was chosen, based on previous reports that have shown that the incident fluence for ONS is relatively independent of pulse duration in the range of 5 $\mu$s to 5 ms.[11] The laser radiation was coupled into a custom-built probe consisting of a 200-$\mu$m-core, low-OH, silica optical fiber with an aspheric lens attached to the distal tip to deliver a collimated, flat-top, 1.1-mm-diam laser spot (corresponding to an area of 0.0095 cm$^2$) at a fixed working distance of 20 mm, as previously reported.[6] The laser spot (1.1-mm-diam) was chosen to be larger than the cavernous nerve (200 to 400 $\mu$m diameter) to simplify alignment of the laser beam on the nerve surface, providing more uniform irradiation and more reproducible stimulation.

Two laser parameters were varied for this study, the laser pulse repetition rate (10 to 100 Hz, cw) and the laser pulse energy (0.28 to 6.37 mJ), which corresponded to an incident fluence of 0.03 to 0.67 J/cm$^2$ for the fixed laser spot diameter. The laser pulse energy was escalated in small increments until the incident fluence reached the threshold for ONS. The ICP response was then measured at or just above the stimulation threshold, providing safe and reproducible stimulation while preventing undesirable thermal damage to the nerve.

The temperature of the CN was also recorded with a thermal camera (A20M, Flir Systems, Boston, Massachusetts) during ONS, in an effort to optimize the laser stimulation parameters and to gain further insight into the mechanism of ONS (Fig. 1).

For each laser dataset, a minimum of five stimulations was performed. The data reported in Table 1 for temperature, and ICP response time represent the average of five independent measurements $\pm$ the standard deviation (SD).

## 3 Results

Table 1 provides a comprehensive summary of the results for our preliminary study of cw versus pulsed ONS. The threshold (minimum) pulse energy, incident fluence, average power, total energy, and temperature for successful ONS are reported, along with the ICP response time. The pulse energy and incident fluence for successful ONS were not fixed as previously thought, but rather decreased significantly as the laser pulse rate was increased. The average power to reach stimulation threshold, however, was not dependent on the pulse rate. Although there was some variation in the results, the ICP response time decreased as the pulse rate was increased from 10 to 100 Hz, with cw irradiation providing the fastest ICP response time. It should be noted that for the 10-Hz dataset, the delayed ICP response actually occurred just after the end of the 15-s laser irradiation time. Finally, successful ONS was observed to be primarily dependent on the time necessary for

**Table 1** Optical nerve stimulation threshold parameters for continuous-wave versus pulsed laser irradiation.

| | Laser pulse repetition rate | | | | | | |
|---|---|---|---|---|---|---|---|
| Parameter | 10 Hz | 20 Hz | 30 Hz | 40 Hz | 50 Hz | 100 Hz | cw |
| Pulse energy (mJ): | 4.84 | 2.57 | 1.71 | 1.34 | 0.94 | 0.56 | NA |
| Incident fluence (J/cm$^2$): | 0.51 | 0.27 | 0.18 | 0.14 | 0.10 | 0.06 | NA |
| Average power (mW): | 48.4 | 51.3 | 51.2 | 53.6 | 47.2 | 55.5 | 47.3 |
| ICP response time (s): | 16.7±1.9 | 14.8±1.3 | 14.5±1.1 | 14.0±0.5 | 12.8±1.3 | 10.9±1.6 | 9.7±0.8 |
| Total energy until stim. (J): | 0.73 | 0.76 | 0.74 | 0.75 | 0.60 | 0.60 | 0.46 |
| Temperature (°C): | 43.8±1.3 | 42.3±1.1 | 42.3±0.2 | 41.5±0.6 | 44.9±1.2 | 44.7±1.2 | 42.9±0.3 |

the nerve to reach a stimulation threshold temperature of 42 to 45 °C, rather than dependent on a specific set of laser parameters.

A representative example of cw optical stimulation of the rat CN is shown in Fig. 3. A strong response in the rat penis was observed with the ICP increasing from a baseline of 16 mmHg to a peak of 39 mmHg. This response occurred approximately 10 s after the laser was turned on, closely corresponding to the time necessary for the CN to heat up above a threshold temperature of approximately 43 °C.

Thermal images of the rat CN before ONS and at peak temperature during ONS are provided in Fig. 4, for the same stimulation parameters and results as shown in Fig. 3. It should be noted that the baseline nerve temperature was not at normal body temperature (37 °C), but rather a few degrees cooler (~34 °C) due to the open surgical model used in these studies (Fig. 1).

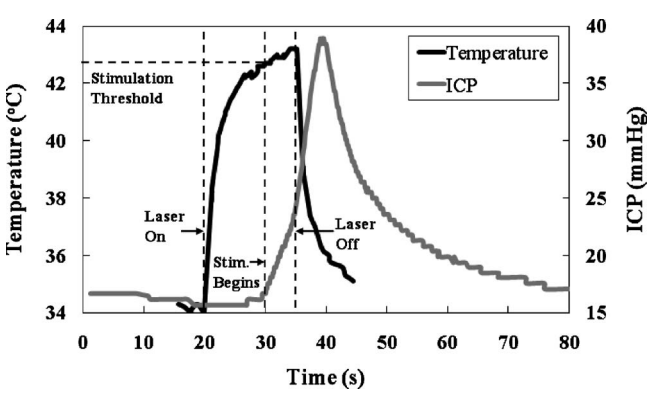


**Fig. 3** Continuous-wave optical stimulation of the rat cavernous nerve (wavelength=1870 nm, spot=1.1 mm, power=47 mW, total energy =0.71 J, and stimulation time=15 s). A delayed response is observed in which the intracavernous pressure (ICP) response in the rat penis begins to increase approximately 10 s after laser irradiation begins (at $t$=20 s) and then continues to increase after laser irradiation ends (at $t$=35 s). The cavernous nerve reaches a stimulation threshold temperature of approximately 43 °C after 10 s of laser irradiation (at $t$ =30 s), closely corresponding to the onset of the increase in ICP.

## 4 Discussion

Previous studies have demonstrated successful ONS using pulsed infrared laser radiation for applications demanding long-term stimulation, as an alternative to conventional ENS. The purpose of this study was to demonstrate short-term ONS using cw infrared laser radiation for producing a more rapid response, necessary for intraoperative diagnostic applications, such as identification of the CNs during prostate cancer surgery. ICP response time decreased significantly as the laser pulse rate increased, and optimal results were observed when the laser was switched to operation in cw mode.

There appears to be a simple explanation for the results summarized in Table 1. cw stimulation produces the fastest ICP response, because delivery of the laser radiation in cw mode also produces the fastest increase in temperature from

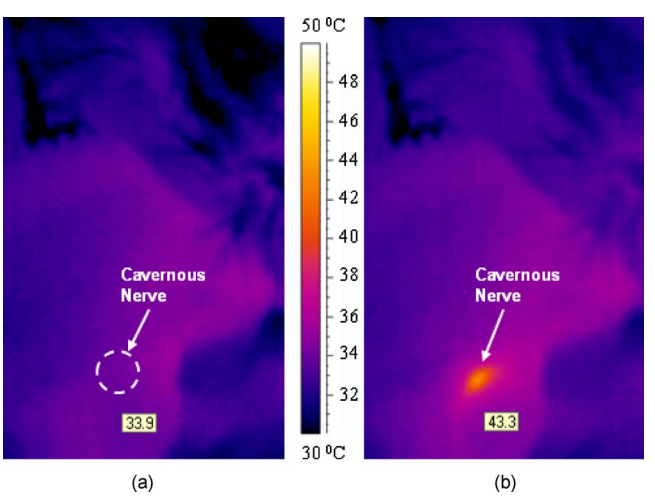


**Fig. 4** Thermal images of the cavernous nerve. (a) Temperature of the nerve just before laser irradiation was at a baseline level of 33.9 °C. (b) The nerve reached a peak temperature of 43.3 °C during laser irradiation, which was just above the nerve stimulation threshold. The orange region showing the peak temperature in the thermal image on the right is approximately the same size as the 1.1-mm-diam laser spot used for heating the cavernous nerve (which has a diameter of 200 to 400 $\mu$m). (Color online only.)

baseline to above the nerve stimulation threshold temperature of approximately 43 °C, as compared to pulsed irradiation with a pulse duration of 5 ms and pulse rates of 10 to 100 Hz.

The results of this study also further confirm that ONS operates primarily based on a photothermal mechanism,[11] in which light energy is converted to heat energy in the nerve until a sufficient amount of heat is generated to increase the nerve temperature above a threshold value (42 to 45 °C) for activation.[12] A strong correlation was observed between the laser irradiation time necessary to raise the nerve temperature above the stimulation threshold and the onset of ICP response, as shown in Fig. 3. Thus, successful ONS was observed to be primarily dependent on the time necessary for the nerve to reach a stimulation threshold temperature for activation, rather than dependent on a specific set of laser parameters.

It should be emphasized that the objective of this study was to produce safe and reproducible ONS using cw infrared laser radiation by operating at or just above the threshold temperature for ONS. It may be possible to achieve an even faster ICP response if the laser power is increased further, so that the time necessary to raise the temperature from baseline to above 43 °C decreases. However, the probability of causing thermal damage to the nerve would also significantly increase if the higher laser power results in excessive elevation of the nerve temperature above a damage threshold of approximately 47 °C.

For a diode-pumped laser (e.g., thulium fiber laser used in this study), operation in cw mode instead of pulsed modulation also translates into a significantly more compact, less expensive laser system for ONS. The advantages of ONS in the cw mode discussed here would also extend to the other diode and fiber laser wavelengths recently tested for optical nerve stimulation,[8,9,11,13] some of which are labeled in Fig. 2.

Finally, although it is well beyond the scope of this study, it should be noted that femtosecond lasers have also been used for successful optical nerve stimulation.[14–16] Laser stimulation using such high intensities and short pulse durations may be mediated by mechanisms fundamentally different than that of the "thermal" lasers operating at low intensities and long pulse durations (or in cw mode). For example, ONS based on low-intensity, long pulse laser irradiation appears to be primarily a photothermal effect from creation of a temporally and spatially mediated temperature gradient at the axon level, which results in direct or indirect activation of transmembrane ion channels causing action potential generation.[11] On the contrary, ONS using high-intensity, short pulsed femtosecond lasers has been attributed to two different mechanisms: 1. a photochemical reaction producing reactive oxygen species adjacent to the cell membrane, and 2. a transient, reversible poration of the cell membrane through perforation of this tissue during laser irradiation.[14] There appears to be considerable disagreement about the mechanism(s) for ONS. Our study utilized low-intensity, long pulse (or cw) laser irradiation and appears to support a photothermal mechanism. In general, laser pulse durations greater than approximately 1 $\mu$s produce a thermal effect in tissue, while shorter pulse durations can involve a nonthermal interaction, so it may be possible that several mechanisms exist and are dependent on the laser parameters used.

## 5 Conclusions

Continuous-wave laser irradiation produces faster optical stimulation of the rat cavernous nerve, as measured by an intracavernous pressure response in the penis, than does pulsed irradiation. This may be important in intraoperative diagnostic applications requiring rapid feedback, such as identification of the cavernous nerves and preservation of erectile function during prostate cancer surgery.

### *Acknowledgments*

This research was supported in part by the Department of Defense Prostate Cancer Research Program, grant number PC073709, and the Department of Energy, grant number DE-FG02-06CH11460.

### *References*

1. J. Wells, C. Kao, E. D. Jansen, P. Konrad, and A. Mahadevan-Jansen, "Application of infrared light for in vivo neural stimulation," *J. Biomed. Opt.* **10**, 064003, 1–11 (2005).
2. L. Klotz, "Neurostimulation during radical prostatectomy: improving nerve-sparing techniques," *Semin Urol. Oncol.* **18**, 46–50 (2000).
3. P. C. Walsh, P. Marschke, W. J. Catalona, H. Lepor, S. Martin, R. P. Myers, and M. S. Steiner, "Efficacy of first-generation Cavermap to verify location and function of cavernous nerves during radical prostatectomy: a multi-institutional study by experienced surgeons," *Urology* **57**, 491–494 (2001).
4. N. M. Fried, S. Rais-Bahrami, G. A. Lagoda, A. Y. Chuang, L. M. Su, and A. L. Burnett, "Identification and imaging of the nerves responsible for erectile function in rat prostate, in vivo, using optical nerve stimulation and optical coherence tomography," *IEEE J. Sel. Top. Quantum Electron.* **13**, 1641–1645 (2007).
5. N. M. Fried, G. A. Lagoda, N. J. Scott, L. M. Su, and A. L. Burnett, "Non-contact stimulation of the cavernous nerves in the rat prostate using a tunable-wavelength thulium fiber laser," *J. Endourol* **22**, 409–413 (2008).
6. S. Tozburun, M. Mayeh, G. A. Lagoda, F. Farahi, A. L. Burnett, and N. M. Fried, "A compact laparoscopic probe for optical stimulation of the prostate nerves," *IEEE J. Sel. Top. Quantum Electron.* **16**, 941–945 (2010).
7. J. D. Wells, S. Thomsen S, P. Whitaker, E. D. Jansen, C. C. Kao, P. E. Konrad, and A. Mahadevan-Jansen, "Optical mediated nerve stimulation: identification of injury thresholds," *Lasers Surg. Med.* **39**, 513–526 (2007).
8. A. D. Izzo, J. T. Walsh, E. D. Jansen, M. Bendett, J. Webb, H. Ralph, and C. P. Richter, "Optical parameter variability in laser nerve stimulation: a study of pulse duration, repetition rate, and wavelength," *IEEE Trans. Biomed. Eng.* **54**, 1108–1114 (2007).
9. A. D. Izzo, J. T. Walsh, Jr., H. Ralph, J. Webb, M. Bendett, J. Wells, and C. P. Richter, "Laser stimulation of auditory neurons: effect of shorter pulse duration and penetration depth," *Biophys. J.* **94**(8), 3159–3166 (2008).
10. G. M. Hale and M. R. Querry, "Optical constants of water in the 200 nm to 200 $\mu$m wavelength region," *Appl. Opt.* **12**, 555–563 (1973).
11. J. Wells, C. Kao, P. Konrad, T. Milner, J. Kim, A. Mahadevan-Jansen, and E. D. Jansen, "Biophysical mechanisms of transient optical stimulation of peripheral nerve," *Biophys. J.* **93**(7), 2567–2580 (2007).
12. P. Cesare, A. Moriondo, V. Vellani, and P. A. McNaughton, "Ion channels gated by heat," *Proc. Natl. Acad. Sci. U.S.A.* **96**, 7658–7663 (1999).
13. R. G. McCaughey, C. Chlebicki, and B. F. Wong, "Novel wavelengths for laser nerve stimulation," *Lasers Surg. Med.* **42**, 69–75 (2010).
14. H. Hirase, V. Nikolenko, J. H. Goldberg, and R. Yuste, "Multiphoton stimulation of neurons," *J. Neurobiol.* **51**, 237–247 (2002).
15. X. Liu, X. Lv, S. Zeng, W. Zhou, and Q. Luo, "Noncontact and nondestructive identification of neural circuits with a femtosecond laser," *Appl. Phys. Lett.* **94**, 061113 (2009).
16. Y. Zhao, X. Liu, W. Zhou, and S. Zeng, "Astrocyte-to-neuron signaling in response to photostimulation with a femtosecond laser," *Appl. Phys. Lett.* **97**, 063703 (2010).

# Continuous-wave Optical Stimulation of the Rat Prostate Nerves using an All-single-mode 1455 nm Diode Laser and Fiber System

Serhat Tozburun[a], Gwen A. Lagoda[b], Arthur L. Burnett[b], and Nathaniel M. Fried[ab*]

[a] Department of Physics and Optical Science, University of North Carolina at Charlotte, NC
[b] Department of Urology, Johns Hopkins Medical Institutions, Baltimore, MD

## ABSTRACT

Optical nerve stimulation (ONS) has recently been reported as a potential alternative to electrical nerve stimulation. Continuous-wave (CW) laser stimulation of the prostate cavernous nerves (CN) in a rat model, *in vivo*, has also been demonstrated in our previous studies. The objective of this study is to present a new all-single-mode-fiber configuration for ONS with the laser operating in CW mode for potential diagnostic applications. An infrared pigtailed single-mode diode laser ($\lambda$ = 1455 nm) was used in this study for noncontact ONS. This new all-fiber approach introduces several advantages including: (1) a less expensive and more compact ONS system, (2) elimination of alignment of optical components, and (3) an improved spatial beam profile. Successful optical stimulation of the rat CN using this new design was observed after the CN reached a threshold temperature of ~ 41 $^{o}$C with response times as short as 3 s. Upon further study, this configuration may be useful for identification and preservation of the cavernous nerves during prostate cancer surgery.

**Key Words:** optical stimulation, nerve, prostate, cavernous nerves, continuous-wave, single-mode, fiber

## 1. INTRODUCTION

Nerve mapping devices utilizing conventional electrical nerve stimulation (ENS) techniques have been used as intra-operative diagnostic tools to assist in preservation of the prostate cavernous nerves (CN) [1-3]. However, these technologies have proven inconsistent and unreliable in identifying the CN and evaluating nerve function. Limitations of ENS in general include: the necessity of physical contact between electrodes and the nerve introducing the potential for mechanical damage; lack of spatial selectivity due to the size limitation of the electrodes; and the presence of electrical stimulation artifacts that may interfere with measurement [4].

Recently, optical nerve stimulation (ONS) using pulsed infrared laser radiation has been reported as a potential alternative to electrical nerve stimulation (ENS) [4-6]. This novel nerve stimulation method offers significant advantages compared with ENS for both scientific and clinical applications. First, it is a non-contact method of stimulation because the infrared laser radiation is delivered in a non-contact mode. Second, spatial selectivity is improved because the laser beam can be focused down smaller than the size of a typical electrode and the problem of electrical current spreading out in the tissue is eliminated for optical nerve stimulation. Finally, when stimulating neural tissue optically, electrical stimulation artifacts are eliminated [4].

In our laboratory, we have studied ONS of the CN in a rat model, *in vivo*, as a pre-clinical model for optical stimulation of the prostate nerves [7-9]. Successful optical stimulation of the rat CN using pulsed and continuous-wave (CW) infrared laser radiation has been previously reported. CW infrared laser radiation during optical stimulation of neural tissue results in faster deposition of energy into the nerve and produces a faster ICP response, thus allowing the use of a less expensive and more compact laser system (e.g., laser diode) for potential diagnostic applications [10]. In all of these previous studies, the experimental setup utilized bulk optical components and multi-mode optical fiber introducing a number of limitations , including: 1. high cost optical components, 2. periodic maintenance for optical alignment and cleaning, and 3. a larger and more expensive ONS system.

*nmfried@uncc.edu; phone: 1 704 687 8149; fax: 1 704 687 8197

In this current study, we demonstrate a new all-single-mode-fiber design approach and the preliminary testing of this approach in a rat CN model, *in vivo*. The results described here define a therapeutic window for safe, reliable**,** and reproducible short-term optical nerve stimulation for identification of the CN.

## 2. MATERIALS AND METHODS

### 2.1 Animal Surgical Preparation

All experiments were performed *in vivo* using six adult male Sprague Dawley rats weighing 400 to 600 g. Care and use of the animals in this study were performed under an approved animal protocol. At the completion of the study, the rats were euthanized by intracardiac injection of potassium chloride while under anesthesia, as is consistent with the recommendations of the Panel of Euthanasia of the American Veterinary Medical Association.

The rats were anesthetized by intraperitoneal injection with 50 mg/kg sodium pentobarbital and secured in the supine position for surgery. The cavernous nerve arising from the ipsilateral major pelvic ganglion situated dorsolateral to the prostate was exposed via a midline suprapubic incision and anterior pelvic dissection. To assess intracavernous pressure (ICP), the shaft of the penis was denuded of skin and the left crural region was cannulated with a 23-G needle connected via polyethylene tubing to a pressure transducer (Harvard Apparatus, Holliston, MA). An increase in ICP after optical stimulation of the CN was detected by a data acquisition system (DI-190, Dataq Instruments, Akron, OH). The response parameters were analyzed with MATLAB software (Mathworks, Natick, MA). Figure 1 shows a photograph of the rat surgical preparation.

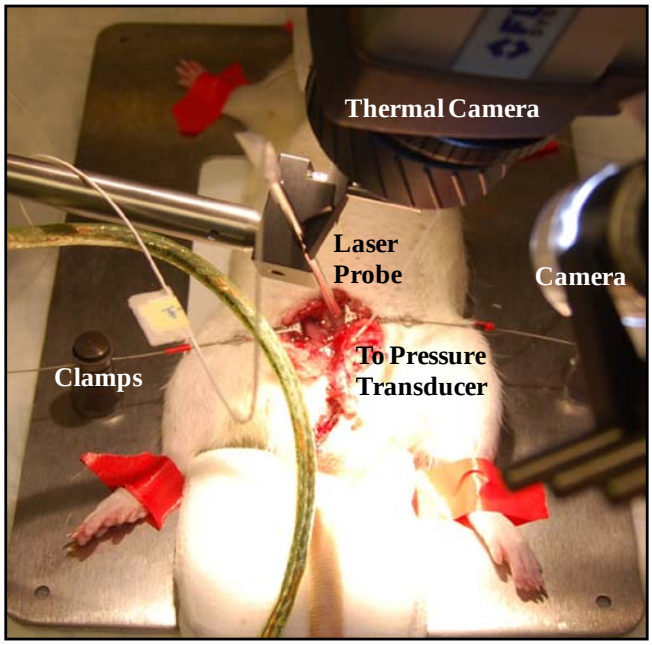


Figure 1. Surgical preparation for optical nerve stimulation.

### 2.2 Experimental Setup

A digital microscope with variable magnification (AD413TL Dino-lite, Torrance, CA) was focused onto the prostate surface to improve alignment of the laser beam with the nerve surface. A thermal camera (A20M, Flir Systems, Boston, MA) provided real-time temperature mapping of the surface of the rat CN during optical stimulation to optimize the stimulation threshold parameters, to identify the upper stimulation threshold for thermal damage, and to gain further insight into the photothermal mechanism of ONS (Figure 1).

A pigtailed single-mode infrared diode laser (QFLD-1450, QPhotonics, L.L.C., Ann Arbor, MI) emitting at a center wavelength of 1455 nm (Figure 2a) was used for optical stimulation of the rat CN. The laser radiation at this

wavelength has an optical penetration depth (OPD) of ~ 350 µm that closely matches the CN dimensions for successful ONS (Figure 2b). This 1455 nm diode represents a more compact and less expensive alternative to the 1870 nm Thulium fiber laser used during our previous ONS studies, but with a roughly similar OPD. It should be noted that Successful pulsed infrared ONS at the wavelength of ~ 1455 nm has been recently reported [11].

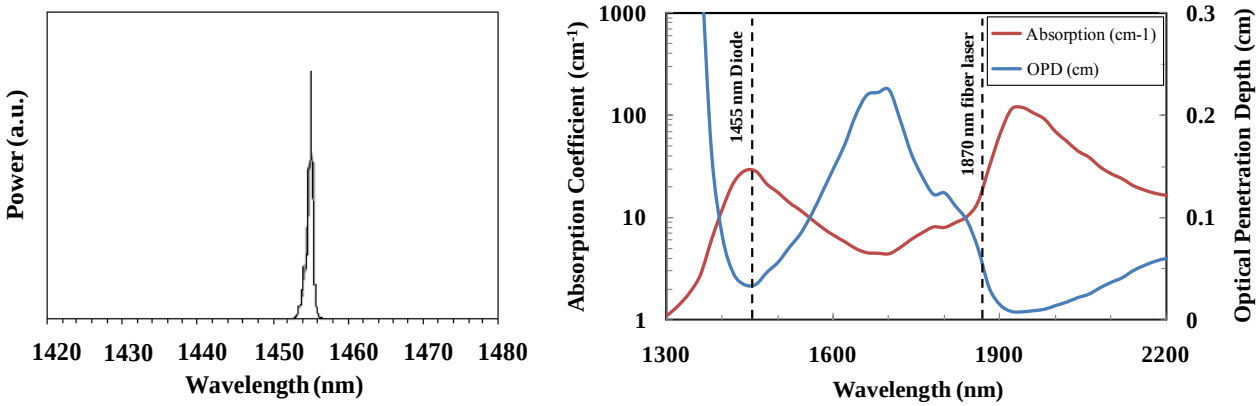


(a) (b)

Figure 2. (a) The emission spectrum of a diode laser operating at a center wavelength of 1455 nm, and (b) the absorption coefficient and optical penetration depth in water as a function of wavelength. The wavelengths of the infrared diode laser used in this study and the fiber laser used in the previous studies are also labeled.

Another visible red diode laser (QFLD-650, QPhotonics, L.L.C., Ann Arbor, MI) with a wavelength of 660 nm was coupled into a single-mode optical fiber and used as an aiming beam to provide alignment. A 9-µm-core single-mode optical fiber coupler with coupling ratio of 10/90 (1x2 SM Dual Window Coupler, Fiber Instrument Sale, Oriskany, NY) was used for combining both the visible and infrared laser beams into a single-mode fiber for delivery. The output of the fiber coupler was connected to a custom-built probe consisting of standard single-mode fiber optic cable (9/125 µm, smf-28+, Corning Optical Fiber, Corning, NY) with an aspheric lens attached to the distal tip for beam collimation. This probe was capable of providing a collimated, 1-mm diameter, Gaussian laser beam over a working distance of ~ 20 mm (Figure 4c). All connections between standard single-mode optical fibers were achieved with FC/APC connectors to prevent back-reflections. Figure 3 provides a diagram of the experimental setup and details of the optical components.

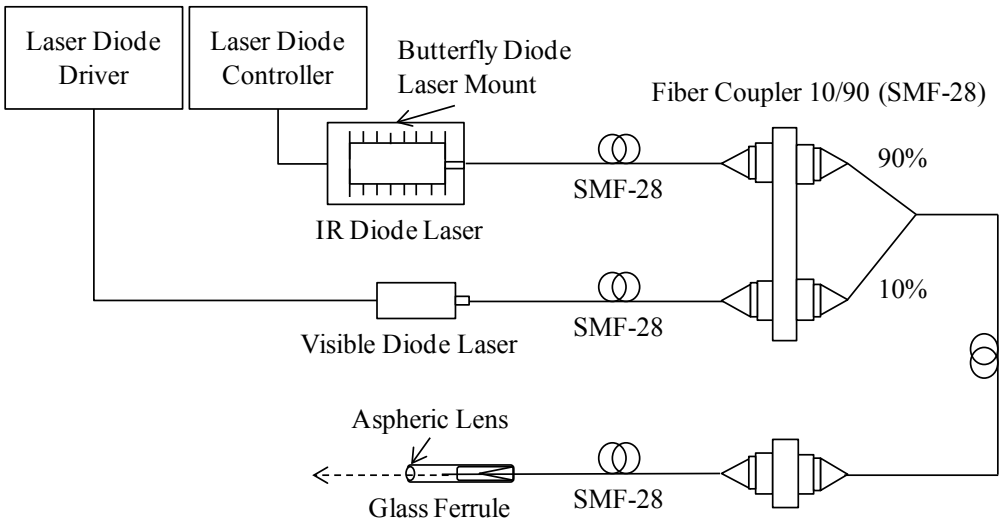


Figure 3. Diagram of experimental setup.

### 2.3 Beam Characterization

The spatial beam profile at the output end of the probe is shown in Figure 4. The 2D and 3D images of the beam profile (Figure 4a and b) were acquired with an infrared beam analyzer (Pyrocam III, Spiricon, Logan UT). Razor blade scans were also performed at different working distances from the distal probe tip to measure the degree of beam collimation (Figure 4c).

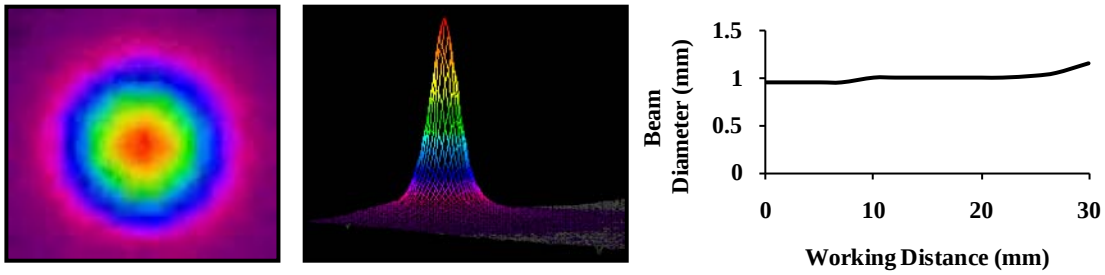


(a) (b) (c)

Figure 4. (a,b) Spatial beam profile in 2D and 3D taken with an infrared beam analyzer. (c) Beam diameter remains at ~ 1 mm diameter over a short working distance of 20 mm.

The data reported in Table 1 for minimum stimulation threshold values, the upper end of the stimulation threshold values and the fastest ICP response time obtained during optical stimulation of the rat CN represents the average of twenty independent measurements ± the standard deviation.

## 3. RESULTS

A summary of the ONS results is provided in Table 1. Successful optical stimulation of the rat CN was achieved at nerve temperatures of 41.3 ± 1.3 $^{o}$C and average laser output powers of 28.3 ± 5.2 mW. The experimental results also implied that there was an upper stimulation threshold temperature of 48.5 ± 1.1 $^{o}$C corresponding to a laser output power of 55.0 ± 7.5 mW for thermal damage to the nerve. Finally, it should be noted that ICP response times as short as ~ 3 s were recorded during a total optical stimulation duration of 15 s.

Table 1. A summary of ONS parameters and response criteria.

| Parameter | Value |
|---|---|
| Fastest ICP response time (s): | 3.8 ± 0.5 |
| Threshold ICP response time (s): | 12.7 ± 1.0 |
| Threshold average power to stimulate (mW): | 28.3 ± 5.2 |
| Threshold temperature to stimulate ($^{o}$C): | 41.3 ± 1.3 |
| Damage threshold average power (mW): | 55.0 ± 7.5 |
| Damage threshold temperature ($^{o}$C) | 48.5 ± 1.1 |

Figure 5 shows a strong ICP response obtained in the rat penis as an example of CW infrared laser stimulation when the rat CN was irradiated with a laser power above the stimulation threshold but below the thermal damage threshold for a period of 15 s. ICP increased from a baseline of 9.3 mmHg to a peak of 48.1 mmHg during ONS. This response was observed ~ 3 s after laser irradiation began, corresponding to the time necessary to elevate the CN temperature above a threshold temperature of ~ 42.2 $^{o}$C in this experiment. The maximum temperature on the CN surface was measured to be 45.1 $^{o}$C at the end of the stimulation duration, significantly below the damage threshold temperature of ~ 48 $^{o}$C.

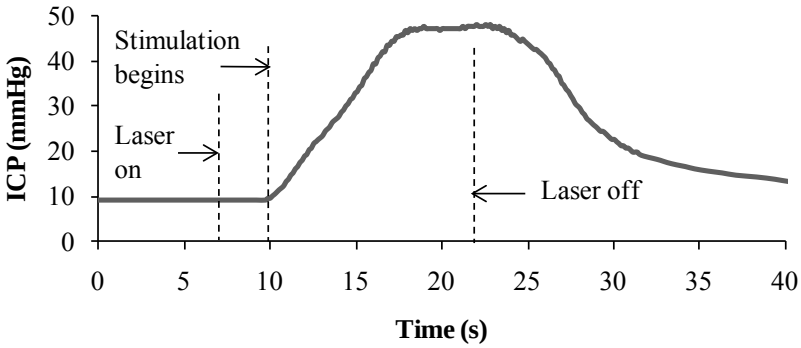


Figure 5. Intracavernous pressure **(ICP)** response as a function of time for optical stimulation of the rat CN (wavelength = 1455 nm, spot diameter = 1 mm, power = 50 mW, total energy = 0.75 J and stimulation time = 15 s).

Photographs of the rat CN taken with a digital microscope before and after optical stimulation are provided in Figure 6. The CN surface temperature reached a maximum value of ~ 48 $^{o}$C during 15 s stimulation duration. Visible thermal damage was observed on the nerve surface as shown in Figure 5b. These results shown here define the upper temperature limit for safe ONS of the rat CN with CW infrared laser radiation.

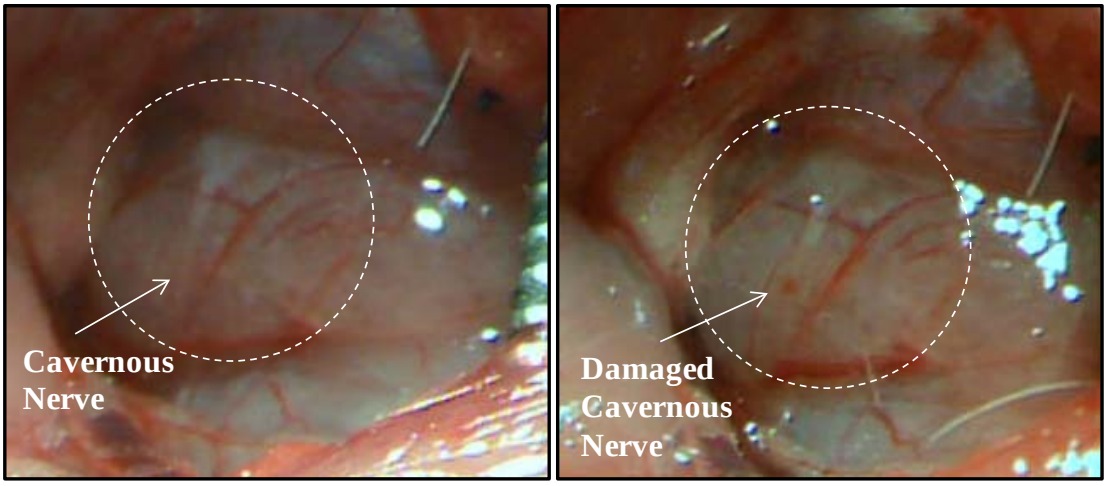


Figure 6. (a) Photographs of the healthy CN before ONS and (b) visible thermal damage after optical stimulation as a result of laser irradiation of the nerve (wavelength = 1455 nm, spot diameter = 1 mm, power = 60 mW, total energy = 0.9 J, and stimulation time = 15 s). The peak tissue temperature reached during ONS was ~ 48 $^{o}$C.

## 4. DISCUSSION

Optical nerve stimulation (ONS) using infrared laser radiation has been previously studied as a potential alternative to electrical nerve stimulation. However, the use of bulk optical components and high-cost infrared lasers (e.g., Holmium:YAG and Thulium fiber lasers) in these studies may represent significant hurdles for translation of ONS into use in the clinic.

This study demonstrates that an all-single-mode-fiber design can be used with an infrared laser for reproducible, safe, short-term, continuous-wave optical stimulation of the prostate cavernous nerves. The results also further confirm that the minimum required nerve temperature for initiating nerve activation is ~ 41 $^{o}$C and that visible thermal damage to the nerve is observed at ~ 48 $^{o}$C, as previously reported [10].

It should be noted that ONS with this all-single-mode-fiber configuration provides several advantages. First, it eliminates the packing complexities encountered during integration of bulk optical components and fiber optics.

Second, it reduces the maintenance and manufacturing costs of the ONS system. Third, delivery of the laser beam through single-mode optical fiber provides an improved spatial beam profile. This may be important for use in beam shaping methods such as conversion of Gaussian to flat-top beam profiles for obtaining a uniform intensity distribution across the nerve surface to avoid hot-spot-induced thermal damage during ONS, and to improve alignment of the laser beam with the nerve.

Finally, analysis of thermal damage to the nerve after laser nerve stimulation was based on nerve function and visible damage on the nerve surface in this study. In future studies, histological analysis of the CN will need to be performed, as a more rigorous indicator of thermal damage. Chronic rat studies to determine whether there are any delayed thermal effects to the nerve will also need to be conducted.

## 5. CONCLUSIONS

An all-single-mode-fiber design for optical stimulation of the rat cavernous nerve, using CW infrared laser radiation, was successfully tested. This approach has several advantages including: lower cost, elimination of alignment and maintenance issues, and improved spatial beam profile. With further development, this ONS system may be useful for safe and reproducible optical stimulation of the cavernous nerves during prostate cancer surgery.

## 6. ACKNOWLEDGMENTS

This research was supported by the DOD Prostate Cancer Research Program, grant number PC073709 and the Department of Energy, grant number DE-FG02-06CH11460.

## REFERENCES

[1] Klotz, L., "Neurostimulation during radical prostatectomy: Improving nerve-sparing techniques," Semin. Urol. Oncol., 18, 46-50 (2000).

[2] Kim, H. L., Stoffel, D. L., Mhoon,D. A., and Brendler, C. B., "A positive caver map response poorly predict recovery of potency after radical prostatectomy," Urology 56, 561-564 (2000).

[3] Walsh, P. C., Marschke, P., Catalona, W. J., Lepor, H., Martin, S., Myers, R. P., and Steiner, S., "Efficacy of first-generation Cavermap to verify location and function of cavernous nerves during radical prostatectomy: A multi-institutional study by experienced surgeons," Urology, 57, 491-494 (2001).

[4] Wells, J., Kao, C., Jansen, E. D., Konrad, P., and Mahadevan-Jansen, A., "Application of infrared light for in vivo neural stimulation," J. Biomed. Opt. 10, 064003, 1-11 (2005).

[5] Wells, J. D., Kao, C., Mariappan, K., Albea, J., Jansen, E. D., Kao, C. C., Konrad, P. E., and Mahadevan-Jansen, A., "Optical stimulation pf neural tissue *in vivo*," Opt. Lett. 30, 504-506 (2005).

[6] Wells, J. D., Thomsen, S., Whitaker, P., Jansen, E. D., Kao, C. C., Konrad, P. E., and Mahadevan-Jansen, A., "Optical mediated nerve stimulation: identification of injury thresholds," Lasers Surg. Med. 39, 513-526 (2007).

[7] Fried, N. M., Rais-Bahrami, S., Lagoda, G. A., Chuang, A. Y., Su, L. M., and Burnett, A. L., "Identification and imaging of the nerves responsible for erectile function in rat prostate, in vivo, using optical nerve stimulation and optical coherence tomography," IEEE J. Sel. Top. Quant. Electron. 13, 1641-1645 (2007).

[8] Fried, N. M., Lagoda, G. A., Scott, N. J., Su, L. M., and Burnett, A. L., "Non-contact stimulation of the cavernous nerves in the rat prostate using a tunable-wavelength thulium fiber laser," J. Endourol. 22(3), 409-413 (2008).

[9] Tozburun, S., Mayeh, M., Lagoda, G. A., Farahi, F., Burnett, A. L., and Fried, N. M., "A compact laparoscopic probe for optical stimulation of the prostate nerves," IEEE J. Sel. Top. Quant. Electron. 16, 941-945 (2010).

[10] Tozburun, S., Cilip, C. M., Lagoda, G. A., Burnett, A. L., and Fried, N. M., "Continuous-wave infrared optical nerve stimulation for potential diagnostic applications," J. Biomed. Opt. 15, 055012, 1-4 (2010).

[11] McCaughey, R. G., Chlebicki, C., and Wong, B. F., "Novel wavelengths for laser nerve stimulation," Lasers Surg. Med. 42, 69–75 (2010).

# Fourier Domain versus Time Domain Optical Coherence Tomography of the Prostate Nerves

Shahab Chitchian[a], Gwen Lagoda[b], Arthur Burnett[b], Nathaniel M. Fried[a,b]

[a] Department of Physics and Optical Science, University of North Carolina at Charlotte, NC
[b] Department of Urology, Johns Hopkins Medical Institutions, Baltimore, MD

## ABSTRACT

Theoretical comparisons of detection performance for Fourier domain (FD) and time domain (TD) optical coherence tomography (OCT) have been previously reported. In this study, we compare several image quality metrics including signal-to-noise ratio (SNR), contrast-to-noise ratio (CNR), and equivalent number of looks (ENL) for TD-OCT and FD-OCT images taken of the rat prostate, *in vivo*. The results show that TD-OCT has inferior CNR, but superior SNR compared to FD-OCT, and that TD-OCT is better for deep imaging of opaque tissues, including the prostate gland.
**Keywords:** prostate, cavernous nerves, optical coherence tomography, OCT, time-domain, Fourier-domain

## 1. INTRODUCTION

OCT is a noninvasive optical imaging technique which can be used to perform high-resolution, cross-sectional *in vivo* and *in situ* imaging of microstructure in biological tissues.[1]

TD-OCT imaging of the cavernous nerves in the rat and human prostate has recently been demonstrated for potential use in laparoscopic and robotic nerve-sparing prostate cancer surgery.[2–4] However, FD-OCT of the prostate has yet to be evaluated.

FD-OCT has been explored over the last decade. It provides superior performance for its high data acquisition rate compared with TD-OCT. However, Brezinski and colleagues[5] have recently reported theoretical analysis that while FD-OCT has some advantages, such as signal integration resulting in faster acquisition rates for potential 3D image reconstruction, its main disadvantage includes poor imaging depth for opaque tissues. They concluded that TD-OCT has superior performance with respect to SNR and penetration depth.

In this study, we compare the results of TD-OCT and FD-OCT imaging of the cavernous nerves in the prostate. SNR and image quality metrics are calculated for the images and discussed in the context of the results previously reported by Brezinski and colleagues.[5,6]

## 2. THEORY AND METHODS

Descriptions of the OCT imaging systems and denoising process are described below, followed by definitions of the image quality metrics used to assess OCT system performance.

### 2.1 TD-OCT vs. FD-OCT

TD-OCT utilizes a Michelson interferometer, relying on interference between a reference and sample broadband optical field. Near-infrared light travels in a reference path, reflecting from a reference mirror, and in a sample path, reflecting from multiple layers within a sample. Refractive index differences among layers in the sample appear as intensity peaks in the interference pattern. Due to the broadband light source, interference occurs between the optical fields when the reference and sample arms optical path lengths are equal or smaller than the coherence length of the light source.[7] Therefore, high-resolution imaging can be achieved.

In the TD-OCT system described above, if the reference path length is fixed and the detection system is replaced with a spectrometer, no moving parts are required to acquire axial scans. The detected intensity

Further author information: (Send correspondence to Shahab Chitchian)
E-mail: schitchi@uncc.edu, Telephone: 1 704 687 8152, Fax: 1 704 687 8197

spectrum is then Fourier transformed into the time domain to reconstruct the depth resolved sample optical structure. FD-OCT has one major advantage that makes it particularly attractive for imaging applications: it obtains entire depth scans in one exposure. Therefore, FD-OCT has the potential to image a given biological sample much more rapidly than TD-OCT, and therefore FD-OCT is also the system of choice for 3D image acquisition. FD-OCT can be performed using a single detector by sweeping the source spectrum using a tunable laser: this method is referred to as swept source (SS) OCT.

There are several differences between TD-OCT and SS-OCT imaging:[6]

First, the power of SS-OCT at any frequency is higher than TD-OCT because of the swept frequencies in small intervals. This results in multiple scattering which is much faster than the power to penetrate deep into the sample. Therefore, both resolution and penetration are degraded. Intensity saturation during SS-OCT also occurs. All frequencies are used in the fast Fourier transform (FFT) to produce the A scan, so central frequency saturation can disturb the entire A scan.

The second difference between TD and SS-OCT is that the reference arm is kept fixed for SS-OCT. Therefore, the frequency sensitivity of the detector is important in imaging deeper tissue structures.

Third, SS-OCT system is a low pass system which reduces performance, because low frequency noise is more deteriorating than in TD-OCT.[5]

The fourth disadvantage of FD-OCT (which includes SS-OCT) compared with TD-OCT is complex conjugate ambiguity. This means that if the point of focus is too close or too far in the tissue, it results in image inversion and loss of resolution, respectively. This is the case when the tissue is moving, for radial imaging, or the image depth is sufficiently large. In the case of moving tissue, any vibrations during the integration time of FD-OCT imaging causes image distortion. This could also be the case when the OCT system is moving.[5]

Fifth, the signal loss from analog to digital (AD) conversion is different for TD and FD-OCT. In a TD-OCT system, digital processing is applied to the analog autocorrelation A scan. Therefore, $log_{10}$ demodulation allows deeper penetration imaging. In a FD-OCT system, the FFT is performed to calculate the A scan from the quantized spectral interferogram. Therefore, the penetration depth of the calculated A scan will be reduced because the logarithmic amplification of the output signal cannot be performed.

### 2.2 OCT Systems

TD-OCT images were acquired in a rat prostate model, *in vivo*, using an endoscopic OCT system (Niris, Imalux, Cleveland, OH) based on an all single-mode fiber common-path interferometer-based scanning system (Optiphase, Van Nuys, CA). An 8 Fr (2.6-mm-OD) probe was used with the OCT system. The system is capable of acquiring real-time images at $200 \times 200$ pixels with 11 $\mu m$ axial and 25 $\mu m$ lateral resolutions in tissue at an acquisition rate of 0.7 frames per second. FD-OCT imaging was performed with a SS-OCT system (OCS1300SS, Thorlabs, Newton, NJ). The FD-OCT images were acquired in real-time at $256 \times 2000$ pixels with 9 $\mu m$ axial and 15 $\mu m$ lateral resolutions in tissue at a rate of 25 frames per second.

### 2.3 Denoising Process

Wavelet shrinkage denoising was previously reported for speckle noise reduction in TD-OCT images of the cavernous nerves.[10] The denoising process for the FD-OCT images was implemented in this study using ImageJ software (NIH, Bethesda, MD) which had better results compared to the wavelet denoising technique.

### 2.4 Image Quality Measurements

Image quality metrics were used to assess performance of the TD-OCT and FD-OCT systems by measuring the average CNR and average ENL over the region of interest (ROI) which is the location of the cavernous nerve in each image. The CNR measures the contrast between an image feature and an area of background noise, while the ENL measures smoothness in areas that should have a homogeneous appearance but are corrupted by speckle. These image quality metrics are measured as[8, 9]

$$CNR_n = 10 \times \log(\mu_n - \mu_b / \sqrt{\sigma_n^2 + \sigma_b^2}) \tag{1}$$

$$ENL_n = \mu_n^2/\sigma_n^2 \tag{2}$$

where $\mu_n$ is the mean of the pixel values in the location of the cavernous nerve, $\sigma_n$ is the pixel standard deviation, and $\mu_b$ and $\sigma_b$ are the pixel mean and standard deviation of a background region of the image, respectively. All measurements are made after logarithmic transformation.

In addition, the global SNR is calculated as[8]

$$SNR = 10 \times \log(\max(X_{lin})^2/\sigma_{lin}^2) \tag{3}$$

where $X_{lin}$ is the two dimensional matrix of pixel values in the OCT image and $\sigma_{lin}^2$ is the noise variance, both on linear intensity scales.

## 3. RESULTS AND DISCUSSION

Nine sample images of the cavernous nerves at different orientations (longitudinal, oblique, and cross-sectional) along the surface of the rat prostate were acquired using TD and FD-OCT systems. Fig. 1(a,c,e) shows the denoised TD-OCT images of the cavernous nerves and prostate. Representative histologic sections were processed for comparison, Fig. 1(b,d,f). Fig. 2 corresponds to the FD-OCT images before and after denoising.

The values of CNR, ENL and SNR for nine FD-OCT and TD-OCT images are shown in Table 1. The values were measured for both original and denoised images. These values for TD-OCT images were previously reported and are shown again here for comparison.[10] An unpaired t-test was performed for comparison of FD-OCT and TD-OCT images with statistical significance given by values of $P < 0.05$. Comparison of original images results in $P$ values for CNR, ENL and SNR of 0.4171, 0.0001 and 0.0001, respectively. Comparison of denoised images results in $P$ values for CNR, ENL and SNR of 0.0142, 0.0491 and 0.0073, respectively. All values are considered to be statistically significant, with the exception of original CNR.

CNR corresponds to the ability to distinguish between ROI which is the location of the cavernous nerve, and the surrounding tissue in the OCT images. The mean values of CNR show that FD-OCT provides better results to differentiate the cavernous nerves from the prostate gland. However, the segmentation algorithm previously introduced by Chitchian et al.[11] overcomes this limitation and provides automatic identification of the cavernous nerves for TD-OCT imaging.

ENL measures smoothness in the areas of ROI. TD-OCT performs better in this respect. SNRs are also better for TD-OCT compared to FD-OCT both before and after denoising. This confirms the studies by Brezinski et al.[5,6] that while FD-OCT has some significant advantages such as faster acquisition rates, its disadvantages of low SNR and penetration depth represent significant limitations for imaging opaque tissues, including the prostate gland.

Fig. 1 also shows that TD-OCT is capable of imaging deeper in the prostate gland and, furthermore, using an edge detection technique,[12] structures deeper in the tissue may be enhanced. However, because of the use of FFT to produce the A scan in FD-OCT imaging, edge detection cannot be applied with FD-OCT.

While SS-OCT has a faster data acquisition rate, its performance is reduced compared to TD-OCT. Because of low frequency noise vulnerability, the results of speckle denoising are less effective for SS-OCT compared to TD-OCT, Fig. 2. Finally, the glandular structure in the prostate FD-OCT images has been distorted compared to the histology, Fig. 2. A possible explanation for this artifact is that central frequency saturation can distort the entire A scan in FD-OCT imaging because all of the frequencies are used in the FFT to produce the A scan.

## 4. CONCLUSION

TD-OCT has distinct advantages for imaging opaque tissues, such as the prostate gland, in applications where imaging penetration depth is important. Denoising is also more effective for TD-OCT compared to FD-OCT with respect to SNR.

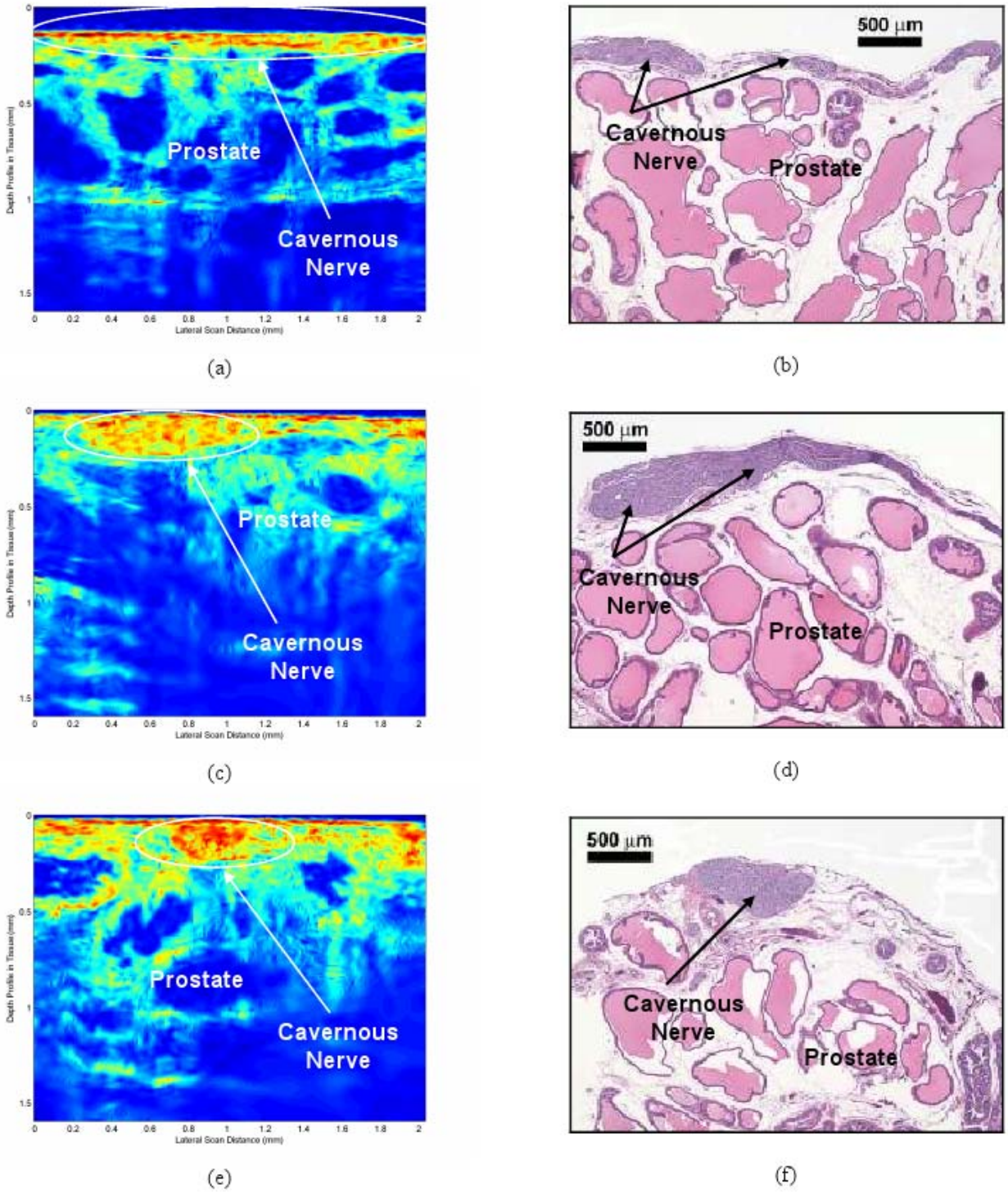


Figure 1. TD-OCT and corresponding histologic images of the rat cavernous nerve: (a,b) Longitudinal section; (c,d) Oblique section; (e,f) Cross-section. In each section, the cavernous nerve corresponds to a relatively high signal intensity (shown in red), and lies superficial to the prostate.

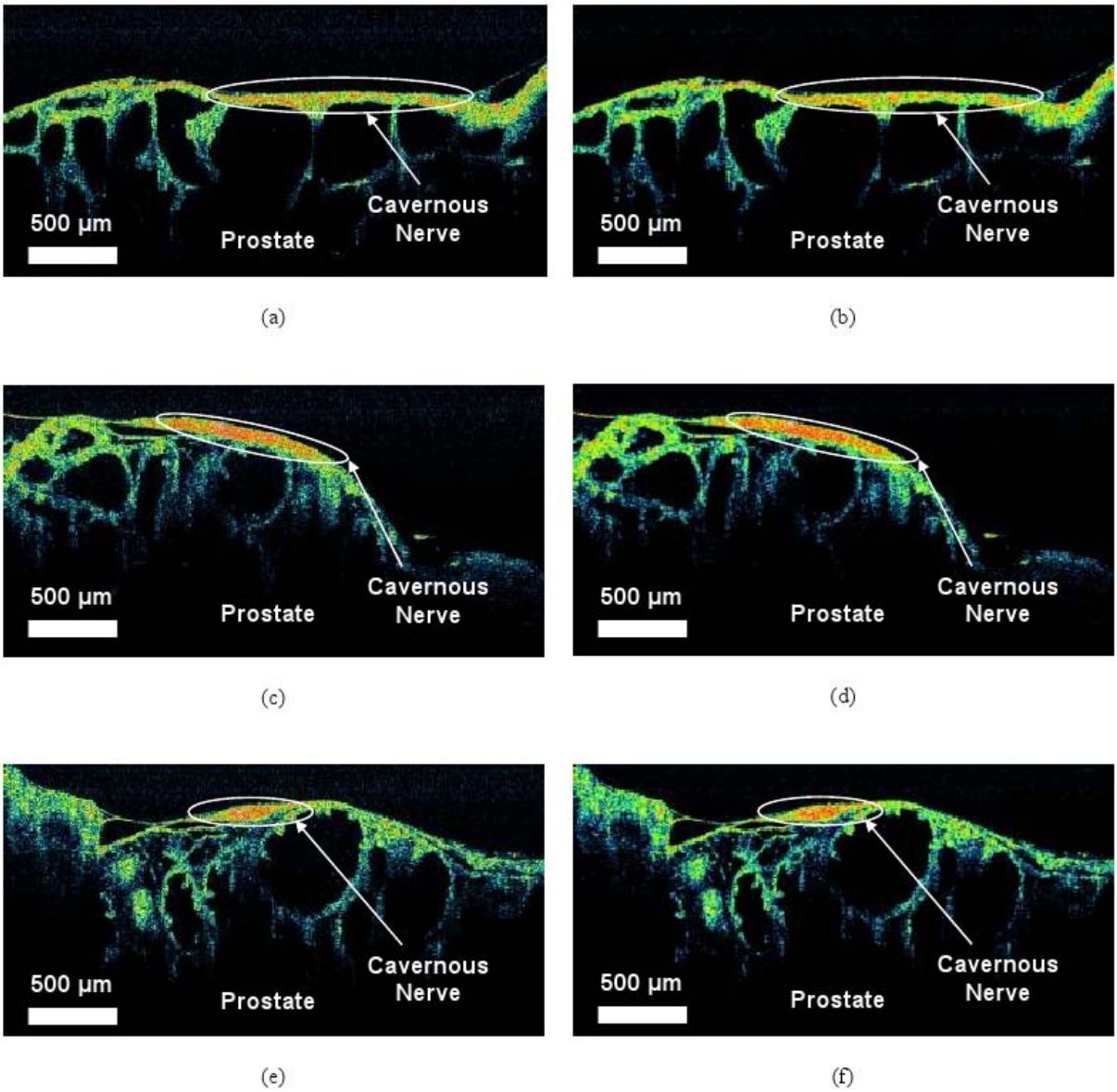


Figure 2. FD-OCT images of the rat cavernous nerve: (a,b) Longitudinal section; (c,d) Cross-section; (e,f) Oblique section. (a,c,e) before; (b,d,f) after denoising.

Table 1. Image quality metrics for FD-OCT and TD-OCT imaging of the prostate gland.

| | | **FD-OCT** | | | **TD-OCT** | | |
|---|---|---|---|---|---|---|---|
| No. | Image | CNR (dB) | ENL | SNR (dB) | CNR (dB) | ENL | SNR (dB) |
| 1 | Original | 9.53 | 59.4 | 23.26 | 3.33 | 1168.6 | 23.36 |
| | Denoised | 17.07 | 1431.2 | 34.15 | 5.63 | 1490.9 | 27.13 |
| 2 | Original | 9.50 | 296.6 | 21.71 | 9.09 | 1420.9 | 27.50 |
| | Denoised | 15.64 | 695.0 | 31.57 | 12.03 | 1932.4 | 45.27 |
| 3 | Original | 10.01 | 100.9 | 23.49 | 9.11 | 1276.9 | 27.99 |
| | Denoised | 17.16 | 630.9 | 34.92 | 11.48 | 1609.9 | 46.06 |
| 4 | Original | 7.58 | 117.9 | 19.96 | 11.96 | 1580.4 | 28.07 |
| | Denoised | 12.23 | 1290.7 | 27.88 | 14.08 | 1866.3 | 35.64 |
| 5 | Original | 10.05 | 102.1 | 23.37 | 7.67 | 1621.7 | 26.76 |
| | Denoised | 17.26 | 1376.2 | 36.71 | 11.39 | 2442.9 | 47.60 |
| 6 | Original | 9.74 | 143.5 | 22.52 | 7.05 | 893.2 | 28.61 |
| | Denoised | 16.07 | 550.3 | 36.54 | 8.86 | 1080.6 | 45.21 |
| 7 | Original | 8.29 | 127.9 | 21.00 | 9.50 | 1974.1 | 25.62 |
| | Denoised | 13.53 | 1671.3 | 33.02 | 13.56 | 2894.8 | 43.90 |
| 8 | Original | 9.08 | 120.9 | 20.77 | 12.44 | 3575.3 | 26.88 |
| | Denoised | 15.10 | 574.4 | 30.18 | 19.32 | 7580.6 | 43.42 |
| 9 | Original | 8.87 | 61.7 | 22.46 | 4.67 | 1014.1 | 25.13 |
| | Denoised | 15.91 | 921.4 | 32.74 | 6.90 | 1303.0 | 33.59 |
| **Mean** | **Original** | **9.18** | **125.6** | **22.06** | **8.31** | **1613.9** | **26.65** |
| | **Denoised** | **15.55** | **1015.7** | **33.08** | **11.47** | **2466.8** | **40.87** |


## Acknowledgments

This research was supported in part by the Department of Defense Prostate Cancer Research Program, Grant #PC073709, and the Department of Energy, Grant #DE-FG02-06CH11460. The authors thank Paul Amazeen and Nancy Tresser of Imalux Corporation (Cleveland, OH) and Tim Villeneuve and Lina Arauz of Thorlabs Inc. (Newton, NJ) for providing the OCT systems used in these studies.


## REFERENCES


[1] D. Huang, E. Swanson, C. Lin, J. Schuman, W. Stinson, W. Chang, M. Hee, T. Flotte, K. Gregory, C. Puliafito, and J. Fujimoto, "Optical coherence tomography," Science **254**, 1178–1181 (1991).

[2] M. Aron, J. Kaouk, N. Hegarty, J. Colombo, G. Haber, B. Chung, M. Zhou, and I. Gill, "Preliminary experience with the niris optical coherence tomography system during laparoscopic and robotic prostatectomy," J. Endourol. **21**, 814–818 (2007).

[3] N. Fried, S. Rais-Bahrami, G. Lagoda, A. Chuang, A. Burnett, and L. Su, "Imaging the cavernous nerves in rat prostate using optical coherence tomography," Lasers Surg. Med. **39**, 36–41 (2007).

[4] S. Rais-Bahrami, A. Levinson, N. Fried, G. Lagoda, A. Hristov, A. Chuang, A. Burnett, and L. Su, "Optical coherence tomography of cavernous nerves: A step toward real-time intraoperative imaging during nerve-sparing radical prostatectomy," Urology **72**, 198–204 (2008).

[5] B. Liu, and M. Brezinski, "Theoretical and practical considerations on detection performance of time domain, Fourier domain, and swept source optical coherence tomography," J. Biomed. Opt. **12**, 044007 (2007).

[6] K. Zheng, B. Liu, C. Huang, and M. Brezinski, "Experimental confirmation of potential swept source optical coherence tomography performance limitations," Appl. Opt. **47**, 6151–6158 (2008).

[7] P. Tomlins, and R. Wang, "Theory, developments and applications of optical coherence tomography," Appl. Phys. **38**, 2519–2535 (2005).

[8] J. Schmitt, S. Xiang, and K. Yung, "Speckle in optical coherence tomography," J. Biomed. Opt. **4**, 95-109 (1999).

[9] D. Adler, T. Ko, and J. Fujimoto, "Speckle reduction in optical coherence tomography images by use of a spatially adaptive wavelet filter," Opt. Lett. **29**, 2878–2880 (2004).

[10] S. Chitchian, M. Fiddy, and N. Fried, "Denoising during optical coherence tomography of the prostate nerves via wavelet shrinkage using dual-tree complex wavelet transform," J. Biomed. Opt. **14**, 014031 (2009).

[11] S. Chitchian, T. Weldon, and N. Fried, "Segmentation of optical coherence tomography images for differentiation of the cavernous nerves from the prostate gland," J. Biomed. Opt. **14**, 044033 (2009).

[12] S. Chitchian, T. Weldon, M. Fiddy and N. Fried, "Combined image processing algorithms for improved optical coherence tomography of the prostate nerves," J. Biomed. Opt. **15**, 046014 (2010).

# Continuous-wave vs. Pulsed Infrared Laser Stimulation of the Rat Prostate Cavernous Nerves

Serhat Tozburun[a], Christopher M. Cilip[a], Gwen A. Lagoda[b], Arthur L. Burnett[b], and Nathaniel M. Fried*[a,b]

[a] Department of Physics and Optical Science, University of North Carolina at Charlotte, NC
[b] Department of Urology, Johns Hopkins Medical Institutions, Baltimore, MD

## ABSTRACT

Optical nerve stimulation has recently been developed as an alternative to electrical nerve stimulation. However, recent studies have focused primarily on pulsed delivery of the laser radiation and at relatively low pulse rates. The objective of this study is to demonstrate faster optical stimulation of the prostate cavernous nerves using continuous-wave (CW) infrared laser radiation, for potential diagnostic applications. A Thulium fiber laser ($\lambda$ = 1870 nm) was used for non-contact optical stimulation of the rat prostate cavernous nerves, *in vivo*. Optical nerve stimulation, as measured by an intracavernous pressure (ICP) response in the penis, was achieved with the laser operating in either CW mode, or with a 5-ms pulse duration at 10, 20, 30, 40, 50, and 100 Hz. Successful optical stimulation was observed to be primarily dependent on a threshold nerve temperature (42-45 $^{o}$C), not an incident fluence, as previously reported. CW optical nerve stimulation provides a significantly faster ICP response time using a laser with lower power output than pulsed stimulation. CW optical nerve stimulation may therefore represent an alternative mode of stimulation for intra-operative diagnostic applications where a rapid response is critical, such as identification of the cavernous nerves during prostate cancer surgery.

**Key Words:** cavernous nerve, laser, optical stimulation, prostate, thulium

## 1. INTRODUCTION

Conventional electrical nerve stimulation (ENS) has several general limitations [1]. First, ENS is limited by the need for physical contact between the electrode and neural tissue, which may result in tissue damage. Second, the spatial precision of ENS is limited by the electrode's size. Third, ENS produces artifacts that may interfere with measurement. Recently, Wells, et al. have developed optical nerve stimulation (ONS) using pulsed infrared laser radiation [1], as an alternative to ENS. They determined that ONS offered several advantages over ENS, including: (1) a non-contact method of stimulation, (2) improved spatial selectivity, and (3) elimination of stimulation artifacts.

Intra-operative electrical nerve mapping devices have been tested as diagnostic tools to assist in identification and preservation of the cavernous nerves (CN) and erectile function during prostate cancer surgery [2]. However, these nerve mapping technologies have proven inconsistent and unreliable in identifying the CN and evaluating nerve function [3]. Therefore, our laboratory has recently begun studying ONS as an alternative to ENS in a rat cavernous nerve model, *in vivo* [4-6]. During initial studies, we focused primarily on the role of laser wavelength, pulse energy, and spatial beam profile on ONS, with less attention spent on the operation mode (e.g. CW vs. pulsed).

Recent ONS studies by other researchers have also focused primarily on the use of laser radiation delivered in pulsed mode and at low pulse repetition rates (2-13 Hz), to avoid thermal build-up and thermal damage to the nerves during long-term stimulation applications [1,7-9]. However, our research group is interested in the potential of ONS to be used as an intra-operative diagnostic tool for identification and preservation of the cavernous nerves during prostate cancer surgery. Practical application of ONS would thus require rapid, short-term nerve stimulation for identification of the cavernous nerves. Therefore, for this current study, we chose to explore delivery of the infrared laser radiation to the nerve at significantly higher pulse rates (10-100 Hz) and in CW mode, with the hypothesis that this method may result in a more rapid response for identification of the cavernous nerves.

*nmfried@uncc.edu; phone: 1 704 687 8149; fax: 1 704 687 8197

## 2. METHODS

### 2.1 Animal Preparation

Seven Sprague Dawley rats (400-600 g) were anesthetized by intraperitoneal injection with 50 mg/kg sodium pentobarbital. The rats were secured in the supine position and prepped for surgery. The cavernous nerve (CN) arising from the ipsilateral major pelvic ganglion situated dorsolateral to the prostate was exposed via a midline suprapubic incision and anterior pelvic dissection (Figure 1). To assess intracavernous pressure (ICP), the shaft of the penis was denuded of skin and the left crural region was cannulated with a 23-G needle connected via polyethylene tubing to a pressure transducer. An increase in ICP after optical stimulation of the CN was detected by a data acquisition system. The response parameters were analyzed with MATLAB software. The ONS experiments were performed under an approved animal protocol, and at the completion of the study, the rats were euthanized by intracardiac injection of potassium chloride while under anesthesia, as is consistent with the recommendations of the Panel of Euthanasia of the American Veterinary Medical Association.

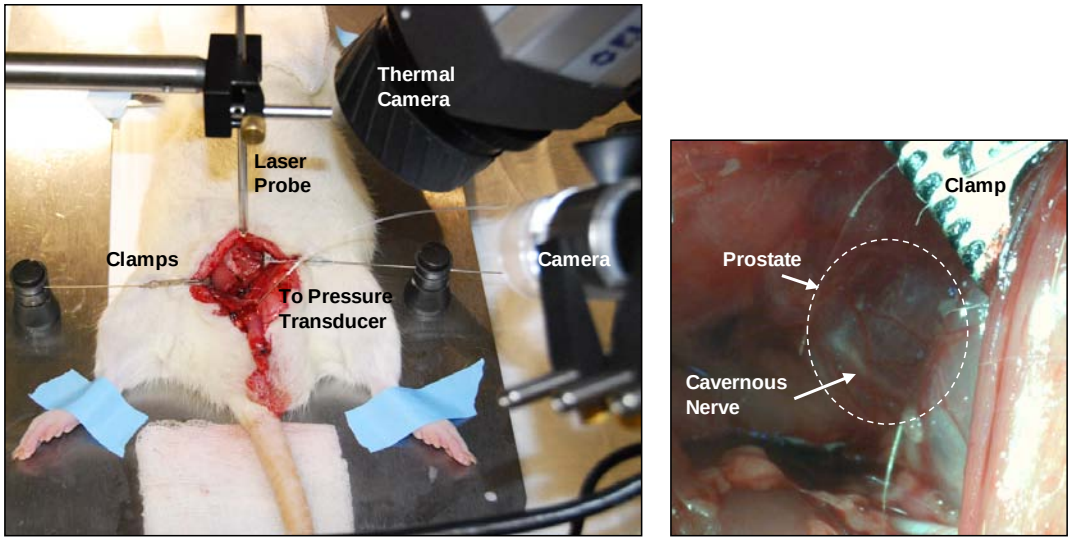


(a) (b)

Figure 1. Experimental setup for optical stimulation of the rat cavernous nerves: (a) Complete setup; (b) Close-up view of the cavernous nerve on the surface of prostate.

### 2.2 Laser Stimulation Parameters

Optical nerve stimulation was performed with a Thulium fiber laser (TLT-5, IPG Photonics, Oxford, MA) using a similar wavelength ($\lambda$ = 1870 nm) and pulse duration (5 ms) as previously reported [6]. The 1870 nm laser wavelength was chosen because it corresponds to an optical penetration depth (OPD) in water, the primary chromophore in soft tissues, of approximately 400 μm (Figure 2) [10], which closely matches the cavernous nerve diameter, for uniform irradiation and stimulation. An OPD significantly less than the nerve diameter would increase the probability of thermal damage to the nerve, and an OPD significantly greater than the nerve diameter would be less efficient for ONS.) A laser pulse duration of 5 ms was chosen, based on previous reports that have shown that the incident fluence for ONS is relatively independent of pulse duration in the range of 5 μs - 5 ms [10]. The laser radiation was coupled into a custom-built probe, consisting of a 200-μm-core, low-OH, silica optical fiber with an aspheric lens attached to the distal tip to deliver a collimated, flat-top, 1.1-mm-diameter laser spot (corresponding to an area of 0.0095 $cm^2$) at a fixed working distance of 20 mm, as previously reported [6]. The laser spot (1.1-mm-diameter) was chosen to be larger than the cavernous nerve (200-400 μm diameter) to simplify alignment of the laser beam on the nerve surface, providing more uniform irradiation and more reproducible stimulation.

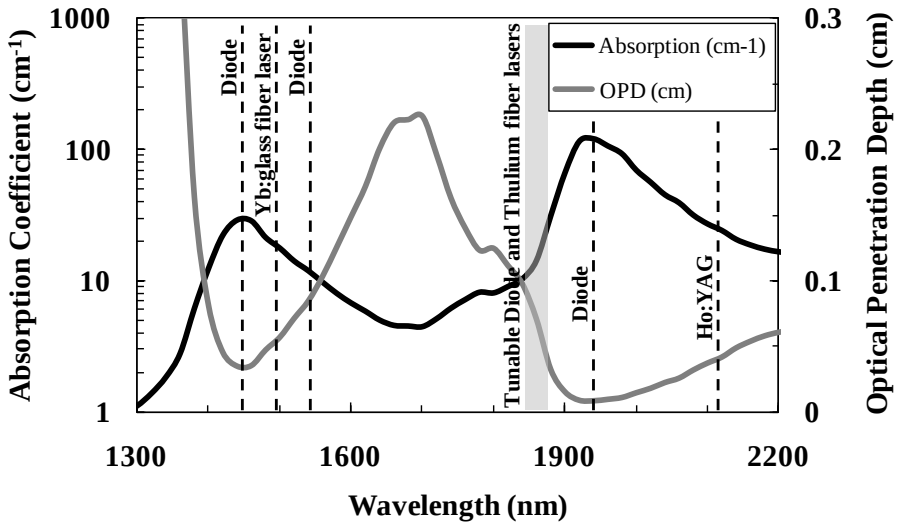


Figure 2. Plot of absorption coefficient and optical penetration depth in water as a function of wavelength. Water is the primary absorber in soft tissues in the near-infrared. The wavelengths of some lasers recently used for ONS are also labeled.

Two laser parameters were varied for this study, the pulse rate (10-100 Hz, CW) and pulse energy (0.28 - 6.37 mJ), which corresponded to an incident fluence of 0.03 - 0.67 J/cm$^2$ for the fixed laser spot diameter. The laser pulse energy was escalated in small increments until the incident fluence reached the threshold for ONS. The ICP response was then measured at or just above the stimulation threshold, providing safe and reproducible stimulation while preventing undesirable thermal damage to the nerve. The CN temperature was also recorded with a thermal camera (A20M, Flir Systems, Boston, MA) during ONS, in an effort to optimize the laser stimulation parameters and to gain further insight into the mechanism of ONS (Figure 1).

### 2.3 Statistical Analysis

For each laser data set, five stimulations were performed. The data reported in Table 1 for temperature, and ICP response time represents the average of five independent measurements $\pm$ the standard deviation (S.D.).

## 3. RESULTS

Table 1 provides a summary of the results for CW vs. pulsed ONS. The threshold (minimum) pulse energy, incident fluence, average power, total energy, and temperature for successful ONS are reported, along with the ICP response time. The pulse energy and incident fluence for successful ONS were not fixed as previously thought, but rather decreased significantly as the laser pulse rate was increased. The average power to reach stimulation threshold, however, was not dependent on the pulse rate. The ICP response time decreased as the pulse rate was increased from 10-100 Hz, with CW irradiation providing the fastest ICP response time. For the 10 Hz data set, the delayed ICP response actually occurred just after the end of the 15 s laser irradiation time. Finally, successful ONS was observed to be primarily dependent on the time necessary for the nerve to reach a stimulation threshold temperature of 42-45 $^o$C, rather than dependent on a specific set of laser parameters.

**Table 1.** Optical nerve stimulation threshold parameters for continuous-wave versus pulsed laser irradiation.

| | Laser Pulse Repetition Rate | | | | | | |
|---|---|---|---|---|---|---|---|
| **Parameter** | **10 Hz** | **20 Hz** | **30 Hz** | **40 Hz** | **50 Hz** | **100 Hz** | **CW** |
| Pulse Energy (mJ): | 4.84 | 2.57 | 1.71 | 1.34 | 0.94 | 0.56 | NA |
| Incident Fluence (J/cm$^2$): | 0.51 | 0.27 | 0.18 | 0.14 | 0.10 | 0.06 | NA |
| Average Power (mW): | 48.4 | 51.3 | 51.2 | 53.6 | 47.2 | 55.5 | 47.3 |
| ICP Response Time (s): | 16.7 ± 1.9 | 14.8 ± 1.3 | 14.5 ± 1.1 | 14.0 ± 0.5 | 12.8 ± 1.3 | 10.9 ± 1.6 | 9.7 ± 0.8 |
| Total Energy until Stim. (J): | 0.73 | 0.76 | 0.74 | 0.75 | 0.60 | 0.60 | 0.46 |
| Temperature ($^o$C): | 43.8 ± 1.3 | 42.3 ± 1.1 | 42.3 ± 0.2 | 41.5 ± 0.6 | 44.9 ± 1.2 | 44.7 ± 1.2 | 42.9± 0.3 |

CW optical stimulation of the rat CN is shown in Figure 3. A strong response in the rat penis was observed with ICP increasing from a baseline of 16 mmHg to a peak of 39 mmHg. This response occurred ~ 10 s after laser was turned on, corresponding to the time necessary for the CN to heat up above a threshold temperature of ~ 43 $^{o}$C.

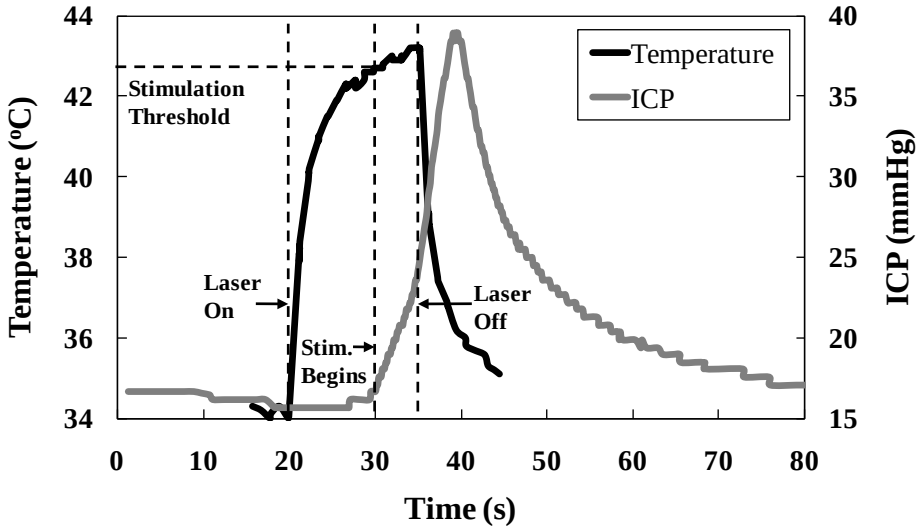


Figure 3. CW stimulation of the rat CN (Wavelength = 1870 nm, Spot = 1.1 mm, Power = 47 mW, Total Energy = 0.71 J, Stimulation Time = 15 s). The ICP response in the rat penis begins to increase ~ 10 s after laser irradiation begins (at t = 20 s) and then continues to increase after laser irradiation ends (at t = 35 s). The cavernous nerve reaches a stimulation threshold temperature of ~ 43 $^{o}$C after 10 s of laser irradiation (at t = 30 s), closely corresponding to the onset of the increase in ICP.

Thermal images of rat CN before ONS and at peak temperature during ONS are provided in Figure 4, for the same stimulation parameters and results as shown in Figure 3. The baseline CN temperature was not at normal body temperature (37 $^{o}$C), but slightly cooler (~ 34 $^{o}$C), due to open surgical model used in these studies (Figure 1).

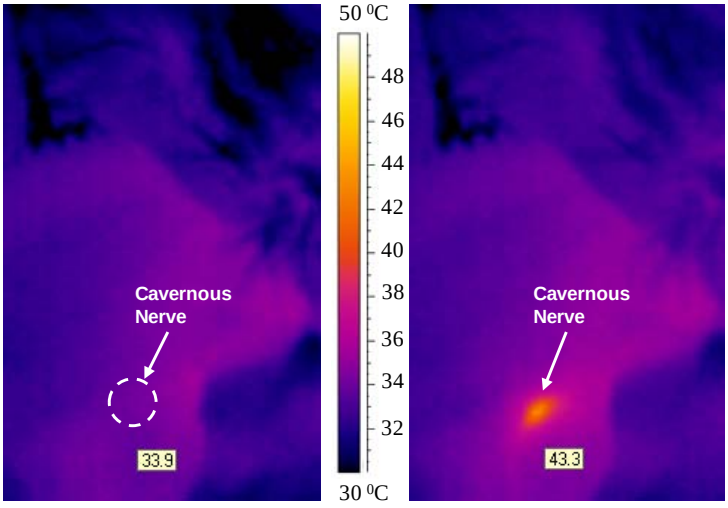


(a) (b)

Figure 4. Thermal images of the CN: (a) Temperature of the nerve just before laser irradiation was at a baseline level of 33.9 $^{o}$C; (b) The nerve reached a peak temperature of 43.3 $^{o}$C during laser irradiation, just above the ONS threshold. The orange region showing the peak temperature in the thermal image on the right is approximately the same size as the 1.1-mm-diameter laser spot used for heating the CN (which has a diameter of 200-400 μm).

## 4. DISCUSSION

Previous studies have demonstrated successful ONS using pulsed infrared laser radiation for applications demanding long-term stimulation, as an alternative to conventional ENS. The purpose of this study was to demonstrate short-term ONS using CW infrared laser radiation for producing a more rapid response, necessary for intra-operative diagnostic applications, such as identification of the CN's during prostate cancer surgery. ICP response time decreased significantly as the laser pulse rate increased and optimal results were observed when the laser was operated in CW mode.

There appears to be a logical explanation for the results summarized in Table 1. CW stimulation produces the fastest ICP response because delivery of the laser radiation in CW mode also produces the fastest increase in temperature from baseline to above the nerve stimulation threshold temperature of ~ 43 $^{o}$C, as compared to pulsed irradiation with a pulse duration of 5 ms and pulse rates of 10-100 Hz.

The results of this study also further confirm that ONS operates primarily based on a photothermal mechanism [11], in which light energy is converted to heat energy in the nerve, until a sufficient amount of heat is generated to increase the nerve temperature above a threshold value (42-45 $^{o}$C) for activation [12]. A strong correlation was observed between the laser irradiation time necessary to raise the nerve temperature above the stimulation threshold and the onset of ICP response, as shown in Figure 3. Thus, successful ONS was observed to be primarily dependent on the time necessary for the nerve to reach a stimulation threshold temperature for activation, rather than dependent on a specific set of laser parameters.

The objective in this study was to produce safe and reproducible ONS using CW infrared laser radiation, by operating at or just above the threshold temperature for ONS. An even faster ICP response may be achieved if the laser power is increased further, so that the time necessary to raise the temperature from baseline to above 43 $^{o}$C decreases. However, the probability of causing thermal damage to the nerve would also significantly increase if the higher laser power results in elevation of the nerve temperature above a damage threshold of ~ 47 $^{o}$C.

For a diode-pumped laser (e.g. Thulium fiber laser used in this study), operation in CW mode instead of pulsed modulation also translates into a significantly more compact, less expensive laser system for ONS. The advantages of ONS in CW mode discussed here would also extend to the other diode and fiber laser wavelengths recently tested for optical nerve stimulation [8,9,11,13], some of which are labeled in Figure 2.

Finally, although it is well beyond the scope of this study, it should be noted that femtosecond lasers have also been used for successful optical nerve stimulation [14-16]. Laser stimulation using such high intensities and short pulse durations may be mediated by mechanisms fundamentally different than that of the "thermal" lasers operating at low intensities and long pulse durations (or in CW mode). For example, ONS based on low intensity, long pulse laser irradiation appears to be primarily a photothermal effect from creation of a temporally and spatially mediated temperature gradient at the axon level which results in direct or indirect activation of transmembrane ion channels causing action potential generation [11]. On the contrary, ONS using high-intensity, short pulsed femtosecond lasers has been attributed to two different mechanisms: (1) a photochemical reaction producing reactive oxygen species adjacent to the cell membrane, and (2) a transient, reversible poration of the cell membrane through perforation of this tissue during laser irradiation [14]. There appears to be considerable disagreement about the mechanism(s) for ONS. Our study utilized low-intensity, long pulse (or CW) laser irradiation and appears to support a photothermal mechanism. In general, laser pulse durations greater than approximately 1 μs produce a thermal effect in tissue, while shorter pulse durations may involve a non-thermal interaction, so it may be possible that several mechanisms exist and are dependent on the laser parameters used.

## 5. CONCLUSIONS

Continuous-wave laser irradiation produces faster optical stimulation of the rat cavernous nerve, as measured by an intracavernous pressure response in the penis, than does pulsed irradiation. This may be important in intra-operative diagnostic applications requiring rapid feedback, such as identification of the cavernous nerves and preservation of erectile function during prostate cancer surgery.

## 6. ACKNOWLEDGMENTS

This research was supported in part by the Department of Defense Prostate Cancer Research Program, Grant# PC073709, and the Department of Energy, Grant# DE-FG02-06CH11460.

## REFERENCES

[1] Wells, J., Kao, C., Jansen, E. D., Konrad, P., and Mahadevan-Jansen, A., "Application of infrared light for in vivo neural stimulation," J. Biomed. Opt. 10, 064003, 1-11 (2005).

[2] Klotz, L., "Neurostimulation during radical prostatectomy: improving nerve-sparing techniques," Semin. Urol. Oncol. 18, 46-50 (2000).

[3] Walsh, P. C., Marschke, P., Catalona, W. J., Lepor, H., Martin, S., Myers, R.P., and Steiner, M.S., "Efficacy of first-generation Cavermap to verify location and function of cavernous nerves during radical prostatectomy: a multi-institutional study by experienced surgeons," Urol. 57, 491-494 (2001).

[4] Fried, N.M., Rais-Bahrami, S., Lagoda, G. A., Chuang, A. Y., Su, L. M., and Burnett, A. L., "Identification and imaging of the nerves responsible for erectile function in rat prostate, in vivo, using optical nerve stimulation and optical coherence tomography," IEEE J. Sel. Top. Quant. Electron. 13, 1641-1645 (2007).

[5] Fried, N. M., Lagoda, G. A., Scott, N. J., Su, L. M., and Burnett, A. L., "Non-contact stimulation of the cavernous nerves in the rat prostate using a tunable-wavelength thulium fiber laser," J. Endourol. 22, 409-413 (2008).

[6] Tozburun, S., Mayeh, M., Lagoda, G. A., Farahi, F., Burnett, A. L., and Fried, N. M., "A compact laparoscopic probe for optical stimulation of the prostate nerves," IEEE J. Sel. Top. Quant. Electron. 16, 941-945 (2010).

[7] Wells, J. D., Thomsen, S., Whitaker, P., Jansen, E. D. Kao, C. C., Konrad, P. E., and Mahadevan-Jansen, A., "Optical mediated nerve stimulation: identification of injury thresholds," Lasers Surg. Med. 39, 513-526 (2007).

[8] Izzo, A. D., Walsh, J. T., Jansen, E. D., Bendett, M., Webb, J., Ralph, H., and Richter, C. P., "Optical parameter variability in laser nerve stimulation: a study of pulse duration, repetition rate, and wavelength," IEEE Trans. Biomed. Eng. 54, 1108-1114 (2007).

[9] Izzo, A. D., Walsh, J. T., Jr., Ralph, H., Webb, J., Bendett, M., Wells, J., and Richter, C. P., "Laser stimulation of auditory neurons: effect of shorter pulse duration and penetration depth," Biophys. J. 94, 3159-3166 (2008).

[10] Hale, G. M. and Querry, M. R., "Optical constants of water in the 200 nm to 200 μm wavelength region," Appl. Opt. 12, 555-563 (1973).

[11] Wells, J., Kao, C., Konrad, P., Milner, T., Kim, J., Mahadevan-Jansen, A., and Jansen, E. D., "Biophysical mechanisms of transient optical stimulation of peripheral nerve," Biophys. J. 93, 2567-2580 (2007).

[12] Cesare, P., Moriondo, A., Vellani, V., and McNaughton, P. A., "Ion channels gated by heat," Proc. Natl. Acad. Sci., USA 96, 7658-7663 (1999).

[13] McCaughey, R. G., Chlebicki, C., and Wong, B. F., "Novel wavelengths for laser nerve stimulation." Lasers Surg. Med. 42, 69-75 (2010).

[14] Hirase, H., Nikolenko, V., Goldberg, J. H., and Yuste, R., "Multiphoton stimulation of neurons," J. Neurobiol. 51, 237-247 (2002).

[15] Liu, X., Lv, X., Zeng, S., Zhou, W., and Luo, Q., "Noncontact and nondestructive identification of neural circuits with a femtosecond laser," Appl. Phys. Lett. 94, 061113 (2009).

[16] Zhao, Y., Liu, X., Zhou, W., and Zeng, S., "Astrocyte-to-neuron signaling in response to photostimulation with a femtosecond laser," Appl. Phys. Lett. 97, 063703 (2010).